



UNIVERSITI
TEKNOLOGI
PETRONAS

**Computational Fluid Dynamics Study on Pressure Drop across a
Duct in Single Rotor Pressure Exchanger**

by

Tan Kien Yoong

15037

Dissertation submitted in partial fulfillment of the requirements for the Bachelor of
Engineering (Hons) (Chemical Engineering)

JANUARY 2015

Universiti Teknologi PETRONAS

Bandar Seri Iskandar

32610

Perak Darul Ridzuan

CERTIFICATION OF APPROVAL

Computational Fluid Dynamics Study on Pressure Drop across a Duct in Single Rotor Pressure Exchanger

by

Tan Kien Yoong

15037

A project dissertation submitted to the
Chemical Engineering Programme
Universiti Teknologi PETRONAS
in partial fulfillment of the requirement for the
BACHELOR OF ENGINEERING (Hons)
(CHEMICAL ENGINEERING)

Approved by,

(Dr. Rajashekhar Pendyala)

UNIVERSITI TEKNOLOGI PETRONAS

BANDAR SERI ISKANDAR, PERAK

January 2015

CERTIFICATION OF ORIGINALITY

This is to certify that I am responsible for the work submitted in this project, that the original work is my own except as specified in the references and acknowledgements, and that the original work contained herein have not been undertaken or done by unspecified sources or persons.

TAN KIEN YOONG

ABSTRACT

The invention of pressure exchanger has made the operating cost of water desalination decreases dramatically by recycling waste pressure back into the system. This will reduce the high pressure pumping capacity of sea water through desalination membrane; hence, reducing the electrical consumption cost, the main contributor of operating cost of a sea water reverse osmosis (SWRO) desalination plant. The practical usage of pressure exchanger in sea water reverse osmosis desalination plant has only been started in the last two decades. As a result, the researches done on pressure exchanger are minimal, especially on the computational fluid dynamics (CFD) study. Limited knowledge is available on the flow patterns inside the pressure exchanger during operation. Numerical study using CFD simulations in ANSYS Fluent 15.0 can provide a better understanding on the fluid dynamics of a single rotor pressure exchanger. This CFD study of single rotor pressure exchanger will focus mainly on the velocity profile of a single duct and calculate pressure drop in a duct from effective velocity in it. The simulation results can provide a platform for researchers to conduct study on the possibility of usage of single rotor pressure exchanger in other fields and applications and also possibility to further enhance this energy recovery device.

ACKNOWLEDGEMENTS

Throughout this project, I have received a lot of assistance from various parties. Without their input and assistance, this Final Year Project would not be successfully completed.

Firstly, I would like to express my deepest gratitude to my very supportive supervisor, Dr. Rajashekhar Pendyala for all his assistance, guidance and advice. Throughout the entire period of this project, he had provided me with many insights of this computational fluid dynamics study of single rotor pressure exchanger. His vast knowledge in the field of CFD had helped me to gain valuable knowledge on pressure exchanger and CFD study. I really appreciate the effort that Dr. Rajashekhar Pendyala has put in my project.

In addition, I would also like to take this opportunity to express my appreciation towards Mr Suhaib Umer Ilyas. He taught me the skills in dissertation and technical paper writing. Besides that, he also gave his opinion and suggestions to me throughout the project period to further improve this Final Year Project.

Lastly, I would like to thank Lim Lian Rui, Wong Yean Sang and Chong Jia Ling who are also doing on CFD study using ANSYS FLUENT 15.0. We helped each other to learn and use this software to obtain better and more accurate result in these two semesters.

TABLE OF CONTENTS

CERTIFICATION OF APPROVAL	i
CERTIFICATION OF ORIGINALITY	ii
ABSTRACT.....	iii
ACKNOWLEDGEMENTS	iv
LIST OF TABLES	vii
LIST OF FIGURES	viii
CHAPTER 1 INTRODUCTION	1
1.1 Background	1
1.2 Types of Pressure Exchanger	2
1.2.1 PX-S Series	2
1.2.2 PX-Q Series	3
1.3 Darcy-Weisbach Equation.....	3
1.4 Problem Statement	4
1.5 Objectives and Scope of Study.....	4
1.6 Relevance and Feasibility.....	5
CHAPTER 2 LITERATURE REVIEW	6
2.1 Pressure Exchanger Development History.....	6
2.2 Operation Principle of Pressure Exchanger.....	7
2.3 Previous Computational Fluid Dynamics Study on Pressure Exchanger.....	8
2.4 Governing Equations	10
2.5 Boundary Conditions.....	13
2.6 Geometry of PX-45S	13
2.7 Darcy-Weisbach Equation.....	15
CHAPTER 3 METHODOLOGY	17
3.1 Research Methodology	17
3.2 Assumptions	17

3.3 Geometry of Model	19
3.4 Technical Data Sheet of Model	19
3.4 Materials Properties.....	20
3.5 Setup Physics.....	21
3.6 Gantt Chart and Key Milestones	23
CHAPTER 4 RESULTS AND DISCUSSION.....	24
4.1 DesignModeler	24
4.2 ANSYS Meshing	28
4.3 ANSYS Fluent.....	32
4.4 Discussion	37
CHAPTER 5 CONCLUSION AND RECOMMENDATIONS	45
5.1 Conclusion.....	45
5.2 Recommendations	45
REFERENCES	
APPENDICES	

LIST OF TABLES

Table 1. Operating conditions of PX-45S [18]	20
Table 2. Performance of PX-45S [18].....	20
Table 3. Properties of Brine and Sea Water [20]	20
Table 4. Input Parameters in ANSYS Fluent	21
Table 5. Gantt chart and key milestones	23
Table 6. Details of Configuration 1 and Configuration 2 in DesignModeler	28
Table 7. Setup Details of ANSYS Meshing	28
Table 8. Statistics of Configuration 1 Meshing	31
Table 9. Statistics of Configuration 2 Meshing	31
Table 10. Pressure drop values for Configuration 1	41
Table 11. Pressure drop values for Configuration 2	42

LIST OF FIGURES

Figure 1. Exterior Design of a PX-S Series Pressure Exchanger [3]	2
Figure 2. Exterior Design of PX-Q Series Pressure Exchanger [4]	3
Figure 3. Cross-sectional view of an operating pressure exchanger [13]	7
Figure 4. Concentration distribution of NaCl in rotor ducts [15]	8
Figure 5. Concentration distribution of NaCl in rotating rotor ducts [15]	9
Figure 6. Graph of volumetric mixing rate against flow in velocity [15]	9
Figure 7. Graph of volumetric mixing rate against rotor speed [15]	10
Figure 8. Methodology flow chart	18
Figure 9. Side view of PX-45S [16]	14
Figure 10. Top view of PX-45S [16]	14
Figure 11. Rotor geometry of PX-45S [15]	19
Figure 12. Isometric View of Configuration 1 of PX-45S Model in DesignModeler	24
Figure 13. Top View of Configuration 1 of PX-45S Model in DesignModeler	25
Figure 14. Isometric View of Configuration 2 of PX-45S Model in DesignModeler	25
Figure 15. Top View of Configuration 2 of PX-45S Model in DesignModeler	26
Figure 16. Position of reference duct in Config. 1 at 0ms, 8ms, 16ms and 23ms	27
Figure 17. Position of reference duct in Config. 2 at 0ms, 8ms, 16ms and 23ms	27
Figure 18. Meshing of Configuration 1 in ANSYS Meshing	29
Figure 19. Meshing of Configuration 2 in ANSYS Meshing	30
Figure 20. Zoom In View of Meshing of PX-45S in ANSYS Meshing	30
Figure 21. Inflated Layer of Meshing in ANSYS Meshing	31
Figure 22. General Setup of ANSYS Fluent	32
Figure 23. Viscous Model of ANSYS Fluent	32
Figure 24. Material Setup (Brine) of ANSYS Fluent	33
Figure 25. Mesh Interfaces	33
Figure 26. Solution Methods	34
Figure 27. Solution Controls	34
Figure 28. Residual Monitors	35
Figure 29. Velocity profile of Configuration 1 at 0ms and 8ms	35
Figure 30. Velocity profile of Configuration 1 at 16ms and 23ms	36
Figure 31. Velocity profile of Configuration 2 at 0ms and 8ms	36
Figure 32. Velocity profile of Configuration 2 at 16ms and 23 ms	37

CHAPTER 1

INTRODUCTION

1.1 Background

Water scarcity has reached a critical level with only less than 1 percent of fresh water is readily accessible for people. Hence, people start to find alternatives to generate fresh water and sea water reverse osmosis (SWRO) desalination is one of the most widely used methods nowadays. Basic SWRO desalination involves pumping ocean water at very high pressures (~75-80barg) across semi-permeable membranes to generate potable water. Concentrated brine with high salt content at high pressure is discharged back into the sea. Traditional SWRO systems use high pressure pumps with high electrical power consumption to pump ocean water across the membranes and discharge waste pressure back into the sea [1].

According to Pique [1], with the invention of pressure exchanger, the problem of high electrical power consumption can be addressed. Pressure exchanger, can also be known as energy recovery device, harness the pressure of the rejected brine and recycle it into the SWRO process before pressurizing the incoming sea water. Therefore, the high pressure pumps do no need to work as hard, which leads to consuming less energy.

Pressure exchanger is introduced less than two decades ago and used in industry for less than 10 years. Therefore, not much literature is available on pressure exchanger. One particular interest field to be researched on pressure exchanger would be fluid dynamics of a pressure exchanger. Therefore, computational fluid dynamics of single rotor pressure exchanger is studied in this project using ANSYS Fluent software. ANSYS Fluent software contains the broad physical modeling capacities required to model flow, heat transfer, turbulence and responses for industrial applications ranging from wind current over an airplane wing to burning in a heater, from bubble segments to oil platforms, from blood stream to semiconductor fabricating, and from clean room outline to wastewater treatment plants [2]. Extraordinary models that give the product the capacity to model in-chamber burning, aero acoustics, turbo machinery, and multiphase frameworks have served to grow its scope.

1.2 Types of Pressure Exchanger

Pressure exchanger is a type of energy recovery device manufactured and patented by Energy Recovery Inc. Due to its high efficiency (>90% energy recovery), pressure exchanger quickly becomes one of the most widely used energy recovery devices in SWRO industry. There are two main series in pressure exchanger: PX-S Series and PX-Q Series. Description on these two series will be available below.

1.2.1 PX-S Series

PX-S Series is well suited for small and large plants. Testing has showed that up to 40 PX devices in parallel can be array in a single train while industrial practice usually put 10 to 16 devices in parallel. The models available for PX-S Series are PX-140S, PX-90S, PX-70S, PX-45S, PX-30S, PX-300, PX-260, PX-220 and PX-180 [3]. Figure 1 shows the exterior design of a PX-S Series pressure exchanger.



Figure 1. Exterior Design of a PX-S Series Pressure Exchanger [3]

1.2.2 PX-Q Series

PX-Q Series are designed for a lifetime with high industrial strength and zero scheduled maintenance. This series is the latest series developed by Energy Recovery Inc. with the aim of higher efficiency and easy installation. The efficiency of PX-Q Series is guaranteed at 97.2% and above. Some of the models in PX-Q Series include PX-Q300 and PX-Q260 [4]. Figure 2 below shows the exterior design of PX-Q Series pressure exchanger.



Figure 2. Exterior Design of PX-Q Series Pressure Exchanger [4]

1.3 Darcy-Weisbach Equation

Pressure drop across the reference duct can be calculated using Darcy-Weisbach equation. The equation is as below [5]:-

$$\Delta P = \lambda \left(\frac{l}{d_h} \right) \left(\frac{\rho v^2}{2} \right) \quad (1)$$

Where,

ΔP = pressure loss (Pa)

λ = Darcy-Weisbach friction coefficient

l = length of duct (m)

d_h = hydraulic diameter (m)

ρ = density (kg/m³)

v = velocity (m/s)

1.4 Problem Statement

With the usage of pressure exchanger in sea water reverse osmosis (SWRO) desalination industry, it is important to understand the fluid dynamics of a single rotor pressure exchanger. However, limited knowledge is available on this field due to the equipment has only been used in industry for less than 20 years.

Available literature on pressure exchanger focuses on cutting energy consumption of a sea water reverse osmosis desalination plant after installation of pressure exchanger [6-8]. It is important to understand the fluid dynamics of the inner part of a pressure exchanger, especially the flow patterns inside the duct of pressure exchanger. The pressure drop across a duct can be calculated from flow patterns inside the duct. Minimizing pressure drop is important in a pressure exchanger as it determines the efficiency of this equipment.

Pressure and velocity contour of a pressure exchanger can be identified through CFD of a pressure exchanger. Hence, by performing a computational fluid dynamics of a single rotor pressure exchanger, the possibility to further enhance the equipment and be used in other industries can be identified.

1.5 Objectives and Scope of Study

The ultimate goal of this project is to study the computational fluid dynamics of a pressure exchanger, especially on the flow patterns inside the pressure exchanger during operation. The study focuses on the fluid flow velocity of brine (rejected sea

water) in a duct. From the flow velocity of brine in a duct, the pressure drop across a duct can be calculated. To further improve this project, two piping configurations have been introduced to study which configuration has a lower pressure drop across a duct.

Therefore, this project will aim to study the computational fluid dynamics of PX-45S, an existing pressure exchanger model developed by Energy Recovery Inc. The objectives of this project are as follows:-

- i. Numerical study of the velocity profile of brine solution in a duct of PX-45 with two different piping configurations.
- ii. To calculate the pressure drop of brine solution in a duct with two different piping configurations using Darcy-Weisbach equation.

1.6 Relevance and Feasibility

The computational fluid dynamics study of pressure drop across a duct in single rotor pressure exchanger is important to understand the flow patterns inside the pressure exchanger during operation. The pressure drop across a duct in pressure exchanger can be calculated using Darcy-Weisbach equation. Pressure drop is an important parameter for pressure exchanger as it determines the efficiency of a pressure exchanger. Hence, this CFD study will compare pressure drop in a duct between two piping configurations.

This project is feasible and relevant to achieve its objectives within time frame given. The overall work flow can be seen in Gantt chart in Chapter 3: Methodology.

CHAPTER 2

LITERATURE REVIEW

2.1 Pressure Exchanger Development History

The idea of recovering waste pressure from water stream can be traced back since the Enlightenment. However, the modern design of a pressure exchanger was developed by Lester Pelton in 1883 for gold mining operations in California [9]. His design used the momentum of water to drive a split buckets wheel. This design was considered a major breakthrough due to its efficient transfer (40-60%) of the water flow from one bucket to another during that time. Turbocharger is another type of pressure exchanger invented in early 1910's to recycle the energy from the gas exhaust in an internal combustion engines. The turbocharger working concept is by capturing the energy of the reject stream with a wheel or turbine. This wheel or turbine is connected to a pump impeller rotating in the feed stream. The efficiency of this device is reported ranged from 50-60% [10].

According to Stover [10], the current pressure exchanger used in SWRO desalination plants works on the principle of positive displacement. Leif J. Hauge invented a rotary pressure exchanger by adapting the concept of rotary positive displacement [11]. Pressure is transmitted from the high-pressure brine stream to fresh sea water stream without any walls between the two streams. This design has only one moving part, which is the rotor.

After several improvements to the design of single rotor pressure exchanger, it was first tested in a pilot plant in Norfolk Harbor, USA in 1994 [12]. The SWRO plant had a capacity of 1500 GPD and it operated continuously for 1000 hours at approximately 33% recovery. This plant had achieved a total of 45-50% reduction in energy consumption after installing an array of pressure exchangers in parallel. The net energy transfer efficiencies of more than 95% have been recorded in this pilot plant. With this experiment of pilot plant in Norfolk, the production of potable water from sea water can size up to 15000 cubic metre per day, which considered to be large plant during that decade.

2.2 Operation Principle of Pressure Exchanger

The principle of operation of a single rotor pressure exchanger can be explained through Figure 3. The central part of this type of pressure exchanger is a rotor with several ducts, usually 12 ducts, of small radius distributed evenly along a circle with larger radius. At any moment, the brine reject fills the right half of a duct and the fresh sea water fills the left. During the first half of the spinning cycle, few ducts are opened to inlet A and outlet B. Brine reject of a fixed volume enters the right end and transmits the high pressure to the feed (fresh sea water). The same volume of sea water is forced out of B, joining the flow towards the membrane for SWRO process. This is then followed by a short amount of time of blockage during which there will be no flow in the duct. In the second half of the spinning cycle, after passing the blockage period, the same duct is now opened to the feed inlet at the left side and to the brine outfall with low pressure at the right side. Fresh sea water enters through inlet C and pushes out the brine reject at D. After passing through a momentarily blockage period again, the same duct is opened at inlet A to receive new brine reject for the second cycle [13, 14].

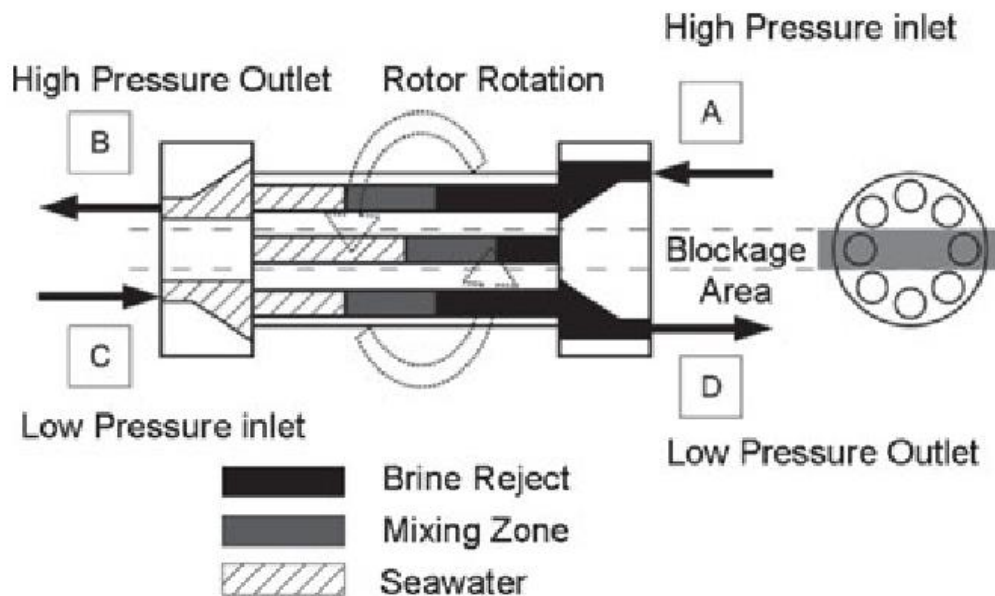


Figure 3. Cross-sectional view of an operating pressure exchanger [13]

2.3 Previous Computational Fluid Dynamics Study on Pressure Exchanger

Zhou *et al.* [15] have conducted a CFD study on the mixing process and the effects of rotary pressure exchanger parameters on the liquid piston on 3D model. This 3D model will describe the dynamics mixing more accurately and closer to real operation conditions. Below are the results obtained from this study. Figure 4 shows the sodium chloride, NaCl concentration distribution in all the rotor ducts. Figure 5 shows the concentration distribution of NaCl in a rotating rotor of pressure exchanger.

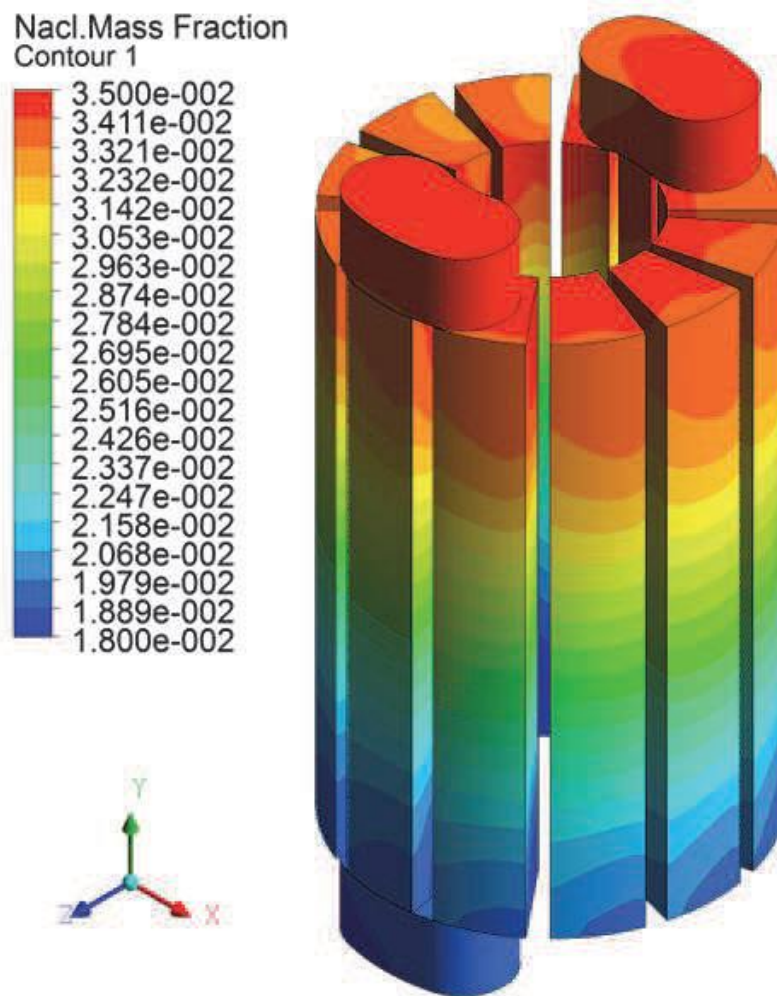


Figure 4. Concentration distribution of NaCl in rotor ducts [15]

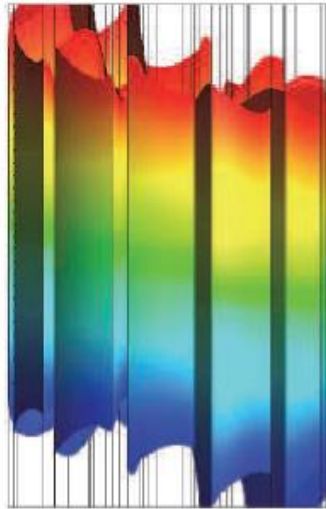


Figure 5. Concentration distribution of NaCl in rotating rotor ducts [15]

The mixing rate of fresh sea water and rejected brine is calculated using equation below.

$$\text{Mixing rate} = \frac{HP_{out} - LP_{in}}{LP_{out} - LP_{in}} \quad (2)$$

Hence, below are the results of mixing rate. Figure 6 shows the relationship of flow in velocity and the volumetric mixing rate when the rotor rotational speed is 1200 rpm. From the graph, it can be clearly seen that the volumetric mixing rate is increasing proportionally with the flow in velocity.

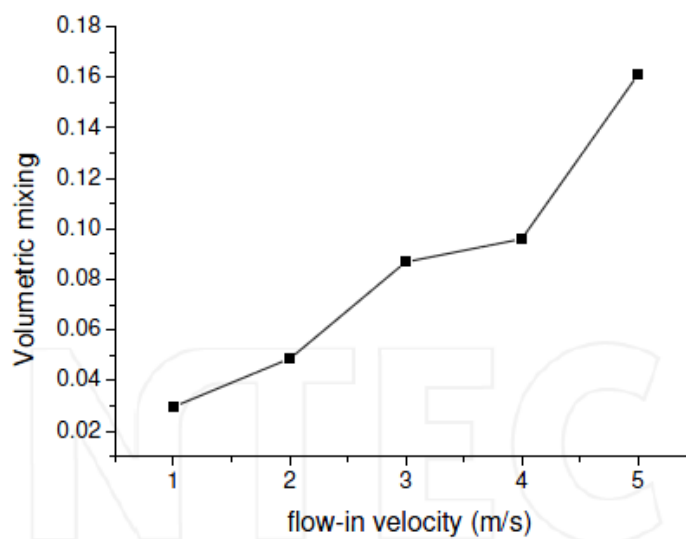


Figure 6. Graph of volumetric mixing rate against flow in velocity [15]

Figure 7 shows the relationship between the rotational rotor speed and volumetric mixing rate when flow in velocity is set at 2.5m/s. The trend of the graph is as rotor speed is increasing, the volumetric mixing rate is decreasing exponentially.

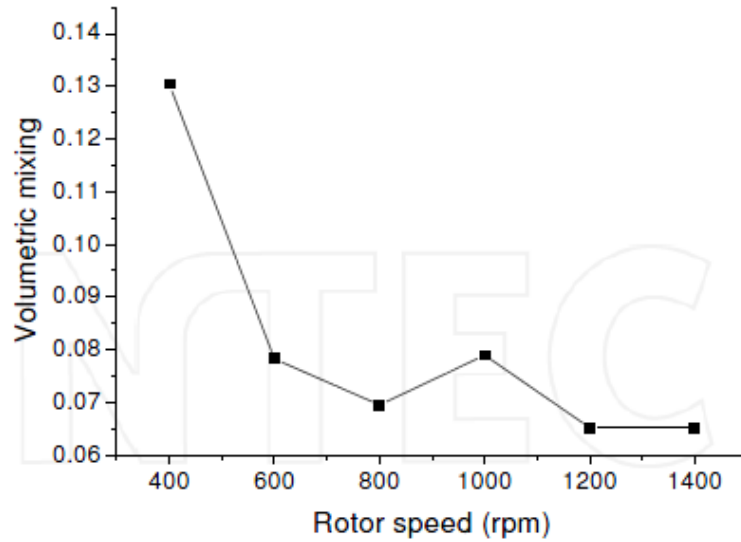


Figure 7. Graph of volumetric mixing rate against rotor speed [15]

2.4 Governing Equations

Numerical simulation of model PX-45S is carried out under cylindrical coordination [15]. Following are the governing equations:-

Continuity equation

$$\frac{\partial \rho}{\partial t} + \nabla \cdot (\rho \vec{v}) = 0 \quad (3)$$

Where,

ρ = density of fluid

t = time

\vec{v} = velocity of fluid in a certain direction

Momentum equation

$$\frac{\partial}{\partial t}(\rho \vec{v}) + \nabla \cdot (\rho \vec{v}\vec{v}) = -\nabla P + \nabla \cdot (\bar{\tau}) + \rho \vec{g} \quad (4)$$

Where,

P = static pressure

$\bar{\tau}$ = stress tensor

$\rho \vec{g}$ = gravitational force.

Stress tensor is given by equation below.

$$\bar{\tau} = \mu \left[(\nabla \vec{v} + \nabla \vec{v}^T) - \frac{2}{3} \nabla \cdot \vec{v} I \right] \quad (5)$$

Where,

μ = molecular viscosity

I = unit tensor.

Specifies equation

$$\frac{\partial}{\partial t}(\rho Y_i) + \nabla \cdot (\rho \vec{v} Y_i) = -\nabla \cdot \vec{J}_i + R_i \quad (6)$$

Where

R_i = net rate of production by chemical reaction.

Since the solutions used are brine reject and fresh sea water, it is assumed that there is no chemical equation during mass transfer. Hence,

$$R_i = 0$$

In turbulent flows,

$$\vec{J}_i = - \left(\rho D_{i,m} + \frac{\mu_t}{Sc_t} \right) \nabla Y_i - D_{T,i} \frac{\nabla T}{T} \quad (7)$$

Where,

Sc_t = turbulent Schmidt number,

$$Sc_t = \frac{\mu_t}{\rho D_t} \quad (8)$$

Where,

μ_t = turbulent viscosity

D_t = turbulent diffusivity.

The default Sc_t is 0.7.

For turbulence model, turbulence kinetic energy is given as below:-

$$\frac{\partial}{\partial t} (pk) + \frac{\partial}{\partial x_i} (pk u_i) = \frac{\partial}{\partial x_j} \left[\left(\mu + \frac{\mu_t}{\sigma_k} \right) \frac{\partial k}{\partial x_j} \right] + G_k + G_b - \rho \epsilon - Y_M \quad (9)$$

Where,

G_b = generation of turbulence kinetic energy due to buoyancy

Y_M = contribution of the fluctuating dilatation in compressible turbulence to the overall dissipation rate.

Turbulent kinetic energy can be simplified to:-

$$\frac{\partial}{\partial t} (pk) + \frac{\partial}{\partial x_i} (pk u_i) = \frac{\partial}{\partial x_j} \left[\left(\mu + \frac{\mu_t}{\sigma_k} \right) \frac{\partial k}{\partial x_j} \right] + G_k + \rho \epsilon \quad (10)$$

Turbulent energy dissipation:-

$$\frac{\partial}{\partial t}(\rho\epsilon) + \frac{\partial}{\partial x_i}(\rho\epsilon u_i) = \frac{\partial}{\partial x_j} \left[\left(\mu + \frac{\mu_t}{\sigma_\epsilon} \right) \frac{\partial \epsilon}{\partial x_j} \right] + C_{1\epsilon} \frac{\epsilon}{k} (G_k + C_{3\epsilon} G_b) - C_{2\epsilon} \rho \frac{\epsilon^2}{k} \quad (11)$$

Where

$$\mu_t = \rho C_\mu \frac{k^2}{\epsilon} \quad (12)$$

The empirical constants for the RNG k-e model for ANSYS Fluent are assigned as following:-

$$C_{1\epsilon} = 1.44, C_{2\epsilon} = 1.92, C_\mu = 0.09, \sigma_k = 1.0, \sigma_\epsilon = 1.3$$

2.5 Boundary Conditions

Boundary condition used for the study is non-slip boundary condition. To simulate the flow at the near-wall region, the standard wall function method is applied. For high pressure brine inlet, velocity- inlet boundary condition is used; for high pressure sea water outlet, pressure outlet boundary condition is used [15].

2.6 Geometry of PX-45S

The geometry of PX-45S is obtained from Energy Recovery Inc, the manufacturer of PX-45S [16]. This model of pressure exchanger will be used to conduct CFD study on single rotor pressure exchanger. The geometry can be referred in Figure 9 and Figure 10 below.

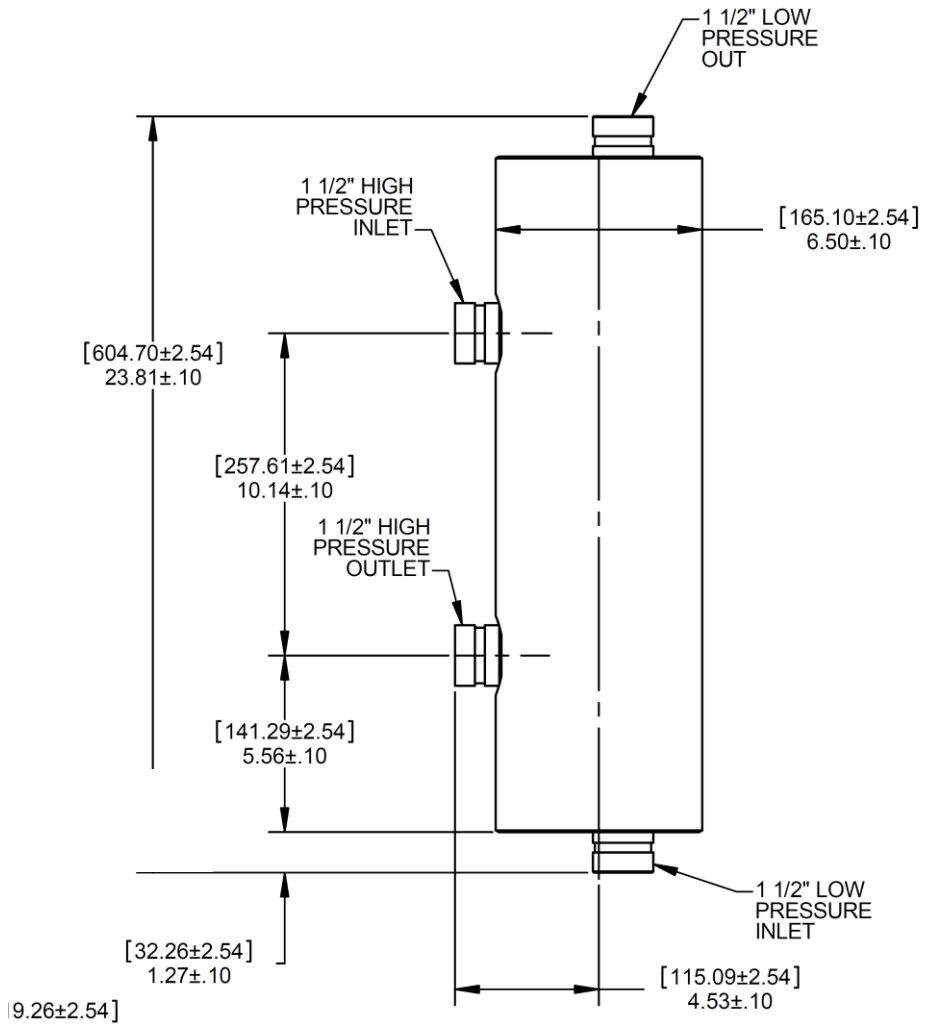


Figure 8. Side view of PX-45S [16]

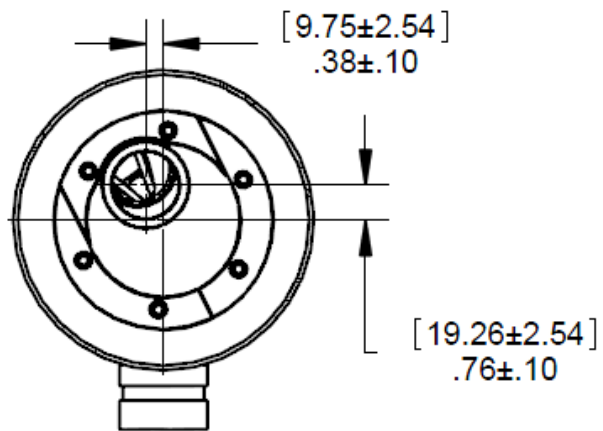


Figure 9. Top view of PX-45S [16]

2.7 Darcy-Weisbach Equation

The flow of fluid through a pipe is resisted by viscous shear stresses of the fluid and the turbulence that occurs along the internal walls of the pipe. This turbulence is created by the roughness of the pipe material. This resistance is usually known as pipe friction and is measured in feet or metres head of the fluid. Hence, the term head loss is also used to express the resistance to flow.

This head loss can be calculated using Darcy-Weisbach equation. The equation is as below [17]:-

$$\Delta P = \lambda \left(\frac{l}{d_h} \right) \left(\frac{\rho v^2}{2} \right) \quad (1)$$

Where,

ΔP = pressure loss (Pa)

λ = Darcy-Weisbach friction coefficient

l = length of duct (m)

d_h = hydraulic diameter (m)

ρ = density (kg/m³)

v = velocity (m/s)

Darcy-Weisbach friction coefficient can be calculated using Colebrook equation as below:-

$$\frac{1}{\lambda^{0.5}} = -2 \log \left[\left(\frac{2.51}{Re \cdot \lambda^{0.5}} \right) + \frac{k}{3.72 d_h} \right] \quad (13)$$

Where,

Re = Reynolds Number

k = roughness of duct (m)

Reynolds number can be calculated as below:-

$$Re = \frac{\rho v d_h}{\mu} \quad (14)$$

Where,

μ = dynamic viscosity (kg/m.s)

Hydraulic diameter can be calculated as below:-

$$d_h = \frac{4A}{p} \quad (15)$$

Where,

A = area section of duct (m²)

p = wetted perimeter of the duct (m)

CHAPTER 3

METHODOLOGY

3.1 Research Methodology

In this project, the computational fluid dynamics of PX-45S is studied using ANSYS Fluent 15.0 software to analyze the velocity profile and pressure drop. ANSYS CFD solvers are based on finite volume method in which the domain is discretized into a finite set of control volumes. General conservation (transport) equations for mass, momentum, energy species, etc. are solved on this set of control volumes. The model used in this CFD study will be 3D model. Figure 8 shows the steps in conducting this study.

3.2 Assumptions

Below are some of the assumptions taken when conducting this CFD study:-

1. The pipes and sleeves of 3D model of pressure exchanger are based loosely on the exact dimension of PX-45S.
2. Pressure exchanger is rotating at 1000rpm. Time step taken to study is every 1ms.
3. The flow in the pressure exchanger will be turbulent.
4. The difference of density and dynamic viscosity between brine and seawater are not large. It is assumed that seawater will behave likely to brine. Hence, brine solution will be the only material in this study.
5. The inlet flow rate is $5\text{m}^3/\text{hr}$ with 80atm initial pressure.
6. No gravitational force acting on the pressure exchanger.

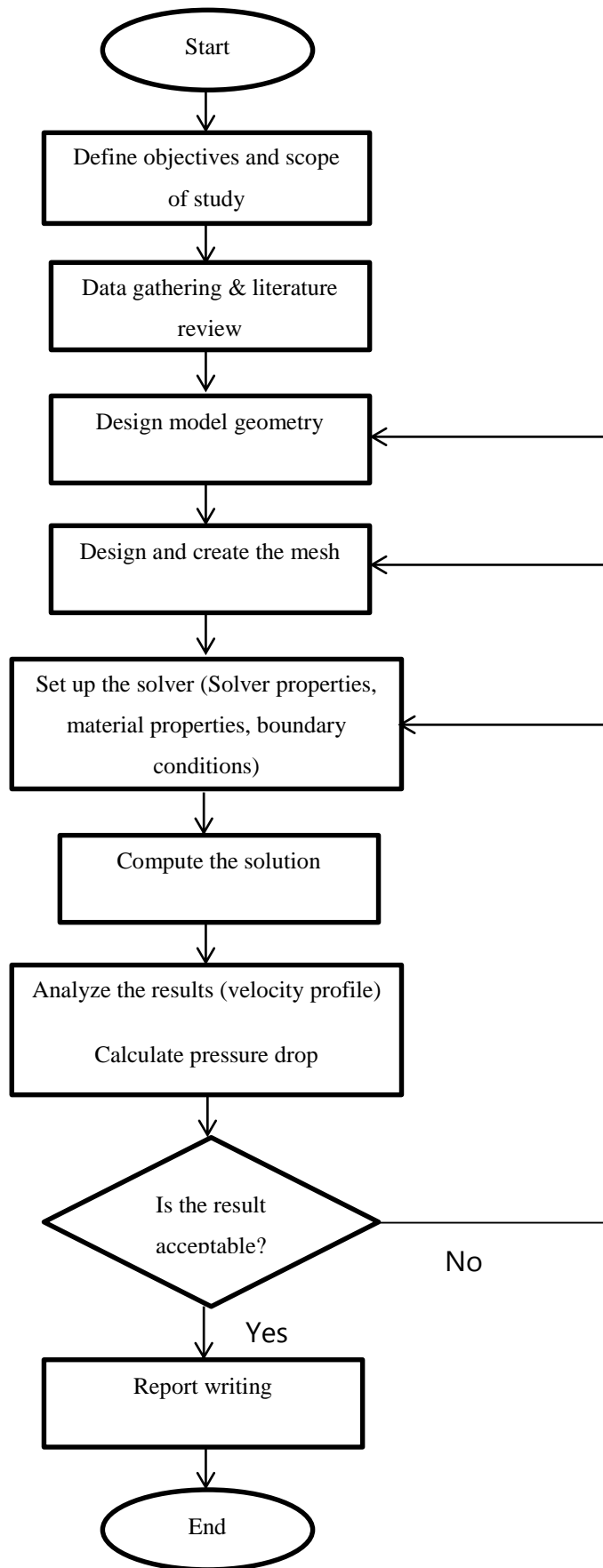


Figure 10. Methodology flow chart

3.3 Geometry of Model

The geometry of the rotor in PX-45S can be referred from Zhou et al. [17]. Figure 11 below is the geometry of rotor of PX-45S from reference.

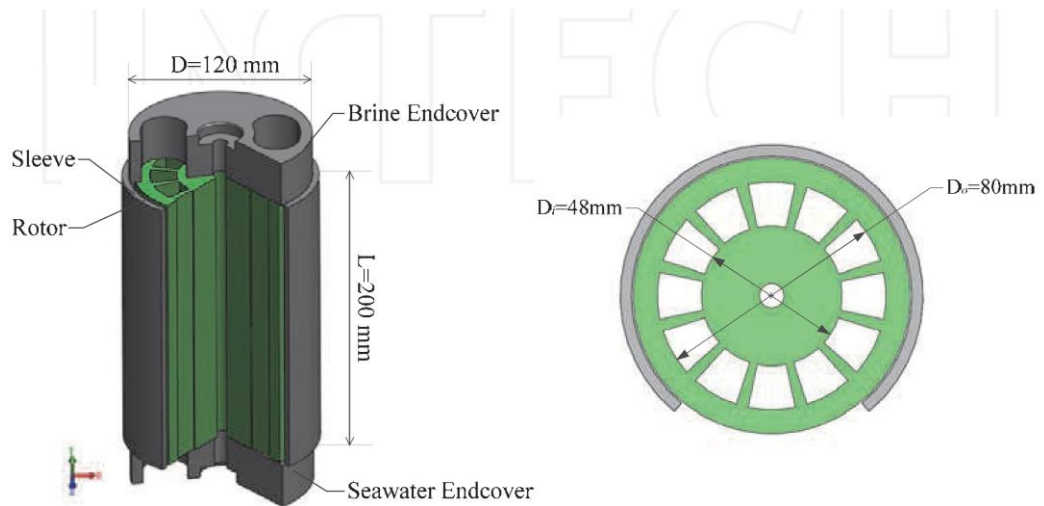


Figure 11. Rotor geometry of PX-45S [5]

3.4 Technical Data Sheet of Model

PX-45S is a new type of pressure exchanger developed by Energy Recovery Inc. This smaller pressure exchanger can cater for both small and large plants by manipulating the number of pressure exchanger in an array. Below is the technical data sheet of PX-45S [15].

Table 1. Operating conditions of PX-45S [15]

Operating Conditions	
Liquid	Seawater
Operating Temperature	33°F-120°F (0.6-49°C)
Maximum Temperature	120°F (49°C)
Specific Gravity	1.03
Viscosity	1.06cP @ 70°F (21.1°C)
Maximum High-Pressure Inlet Flow	45gpm (10m ³ /hr)
Maximum Low-Pressure Inlet Flow	45gpm (10m ³ /hr)
Maximum Inlet Low Pressure	300psig (20.7barg)
Maximum Inlet High Pressure	1200psig (82.7barg)
Minimum Discharge Pressure	14.5psig (1bar)

Table 2. Performance of PX-45S [18]

Performance	
Peak Efficiency	96%
Maximum High Pressure Differential	10psig (0.7bar) @ 45gpm
Maximum Low Pressure Differential	11psig (08bar) @ 45gpm
Maximum Lubrication Flow	2.1gpm (0.5m ³ /hr)
Maximum Rotational Speed	1500rpm
Maximum Salinity Increase at Membranes	5% @ 40% Recovery

3.4 Materials Properties

In this CFD study, the materials used brine with high salinity. The salinity of brine usually ranges from 50 to 75 g/L [18]. Therefore, the salinity of brine is 60g/L at 25°C. Below are the properties required for this study for 60g/L brine solution:-

Table 3. Properties of Brine and Sea Water [18]

Brine	Value
Density (kg/m ³)	1044.1
Dynamic Viscosity (kg/m.s)	0.00114

3.5 Setup Physics

ANSYS Fluent is used to study the computational fluid dynamics of PX-45S single rotor pressure exchanger in this project. Before conducting the simulation, some setup parameters must first be filled. Below are the parameters being setup in ANSYS Fluent:-

Table 4. Input Parameters in ANSYS Fluent

Parameters	Settings	Reason
Solver	<ul style="list-style-type: none"> Type: Pressure-based Time: Steady-state 	<ul style="list-style-type: none"> ➤ Pressure-based type is for incompressible fluid flow in low velocity. ➤ Time is set as steady state to study the velocity profile at given time.
Model	<ul style="list-style-type: none"> Enable viscous k-ϵ Enable standard wall treatment 	<ul style="list-style-type: none"> ➤ Involve turbulence fluid flow velocity on swirl. ➤ Obtain result for both laminar and turbulent flow.
Materials	<ul style="list-style-type: none"> Brine 	<ul style="list-style-type: none"> ➤ Density (1044.1 kg/m^3) and dynamic viscosity (0.00114 kg/m.s) of brine is introduced.
Boundary conditions	<ul style="list-style-type: none"> Velocity-inlet: 5.459 m/s (for inlet pipes) Supersonic/ Initial Gauge Pressure: 80 atm Interface (for pipe-sleeve interfaces and sleeve-ducts interfaces) 	<ul style="list-style-type: none"> ➤ Initial pressure into pipe is 80 atm. ➤ To enable fluid flow from one body to another body
Mesh interfaces	<ul style="list-style-type: none"> Interface between pipe and sleeve Interface between sleeve and ducts 	<ul style="list-style-type: none"> ➤ To enable flow from one geometry to adjacent geometry

Solution methods	<ul style="list-style-type: none"> • Scheme: Simple • Momentum: Second order • Turbulency Kinetic Energy: First order • Turbulent dissipation rate: First order 	<ul style="list-style-type: none"> ➤ Simple scheme is used for velocity and pressure corrections to obtain a more accurate pressure field.
Solution Initialization	<ul style="list-style-type: none"> • Hybrid initialization 	<ul style="list-style-type: none"> ➤ Used for single-phase flow

3.6 Gantt Chart and Key Milestones

Table 5. Gantt chart and key milestones

No.	Progress	Week													
		1	2	3	4	5	6	7	8	9	10	11	12	13	14
1	Evaluating results and improvements	■	■	■	■	■	■	■	■	■	■				
2	Submission of Progress Report								■						
3	Pre-Sedex										■				
4	Final Report Softcopy Draft Submission											■			
5	Submission of Technical Paper											■			
6	Submission of Soft Bound Copy of Final Report												■		
7	Oral Presentation													■	
8	Submission of Hard Bound of Final Report														■

Progress
 Key Milestones

CHAPTER 4

RESULTS AND DISCUSSION

4.1 DesignModeler

By using ANSYS DesignModeler software, the 3D geometry of PX-45S single rotor pressure exchanger is created using the exact dimension of the equipment [19, 20].

The techniques used in developing this model are extrude, pattern and rotate. Extrude is used to develop 3D geometry from a 2D sketch and pattern is used to duplicate bodies with the same geometry. Rotate is used to rotate the duct in each time step. All the bodies in the geometry are chosen as fluid.

Figures below show the geometry model of two different piping configurations, naming Configuration 1 and Configuration 2.

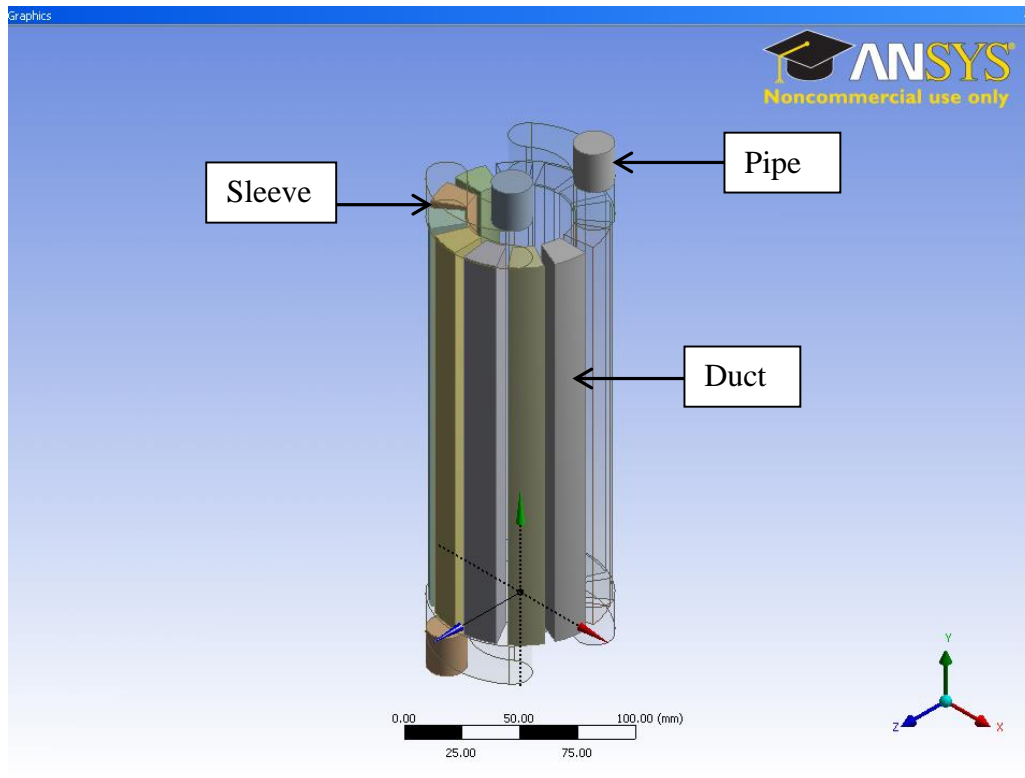


Figure 12. Isometric View of Configuration 1 of PX-45S Model in DesignModeler

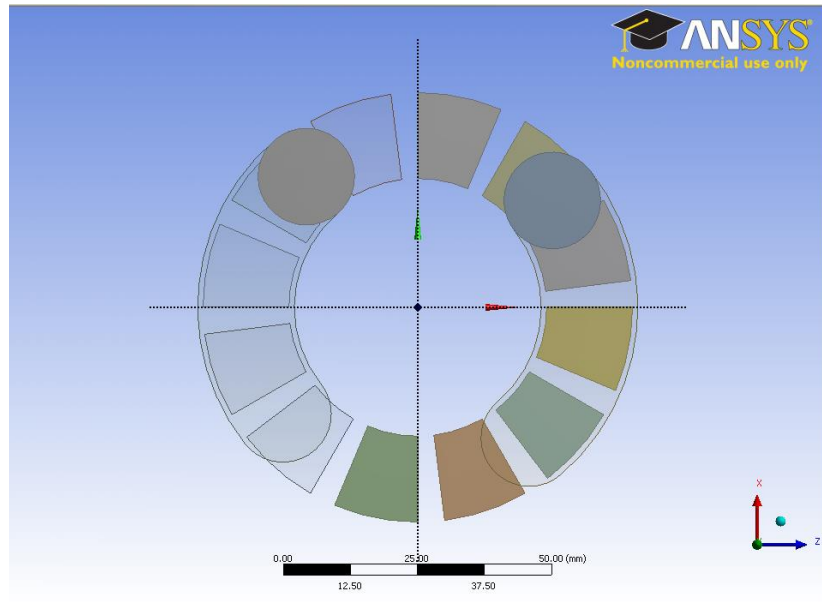


Figure 13. Top View of Configuration 1 of PX-45S Model in DesignModeler

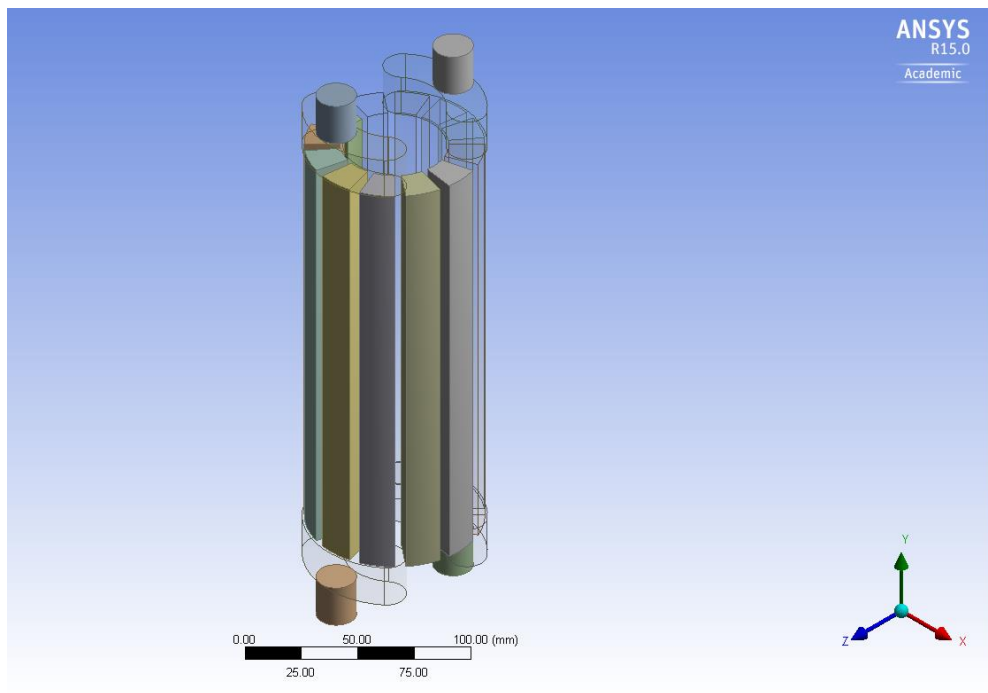


Figure 14. Isometric View of Configuration 2 of PX-45S Model in DesignModeler

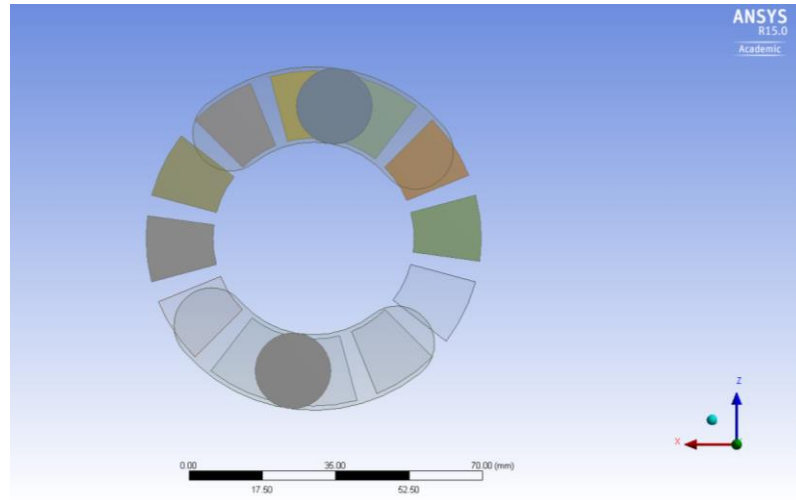


Figure 15. Top View of Configuration 2 of PX-45S Model in DesignModeler

The rotor of PX-45S is rotating at 1000rpm, hence, for every 1 millisecond, the ducts will rotate 6° clockwise. Using this assumption, a reference duct is chosen to conduct this CFD study of pressure drop across a duct. The starting time is set at 0 millisecond when this reference duct touches the sleeve. The end time is at 23 millisecond when the reference duct comes into contact with the sleeve before leaving the interface with the sleeve. Below are the geometry models of Configuration 1 and Configuration 2 at different time (0ms, 8ms, 16ms and 23ms), where the duct highlighted in red box is the reference duct:-

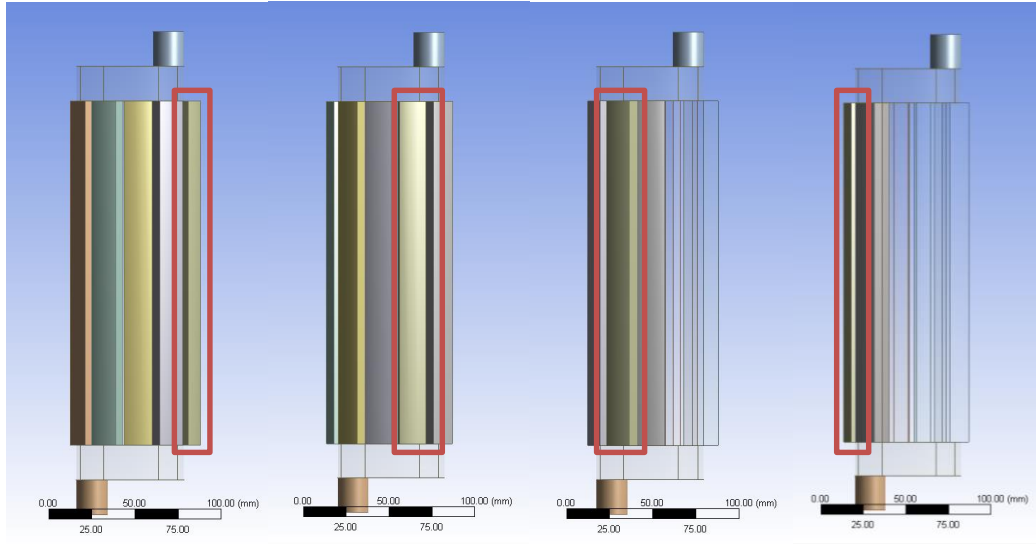


Figure 16. Position of reference duct in Configuration 1 at 0ms, 8ms, 16ms and 23ms

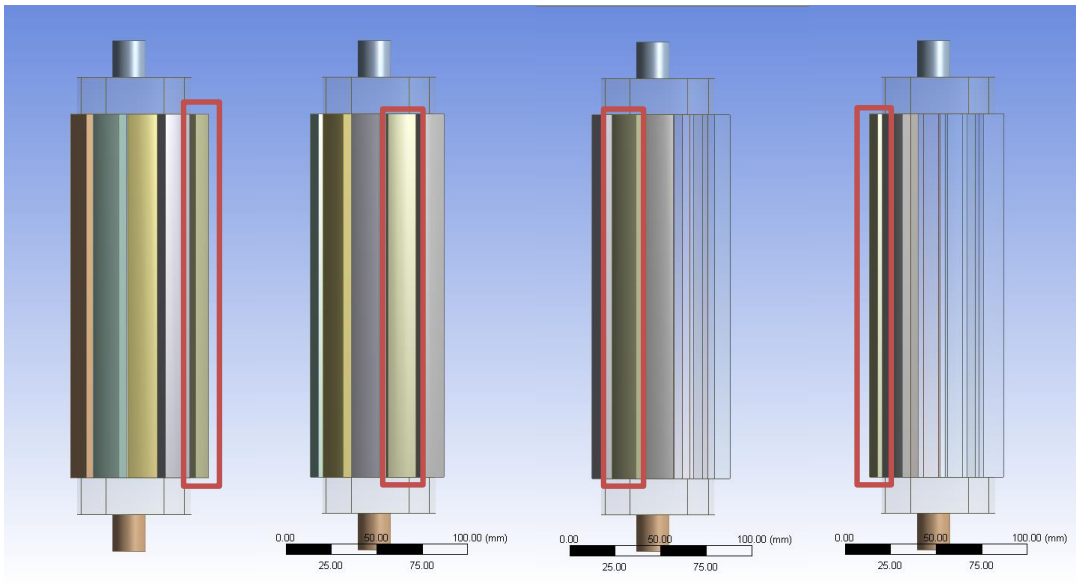


Figure 17. Position of reference duct in Configuration 2 at 0ms, 8ms, 16ms and 23ms

The length unit used in PX-45S model is in millimeter (mm). Below are the details of Configuration 1 and Configuration 2 from DesignModeler:-

Table 6. Details of Configuration 1 and Configuration 2 in DesignModeler

Details	Value
Bodies	20
Volume	6.0046e+005 mm ³
Surface Area	1.7086e+005 mm ²
Faces	108
Edges	200
Vertices	128

Configuration 1 and Configuration 2 of pressure exchanger model have the same details in DesignModeler.

4.2 ANSYS Meshing

After creating 3D geometry using DesignModeler, the geometry is then imported into ANSYS Meshing software to mesh the geometry model. Meshing is one of most crucial part in a CFD study. Too many cells may result in long simulation time to converge and too few cells will result to inaccurate results [15].

Below are some of the important setups for meshing to acquire an acceptable mesh for this project:-

Table 7. Setup Details of ANSYS Meshing

Detail	Setup
Use Advanced Size Function	On: Proximity and Curvature
Relevance Center	Fine
Smoothing	High
Use Automatic Inflation	Program Controlled

In the “Use Advanced Size Function” setup, “On: Proximity” function is suitable for square bodies or long bodies. “On: Curvature” function is suitable for round and curved bodies [16]. Hence, by selecting “On: Proximity and Curvature” in “Use Advanced Size Function”, the mesh can cater for long ducts in the geometry as well as round surfaces (sleeves and pipes).

For “Relevance Center” and “Smoothing”, “Fine’ and “High” setups are chosen respectively. By choosing this setting, ANSYS Meshing will generate a finer and more uniform meshing for the model, hence improving its accuracy in calculation in simulation.

It is important to have inflation layer near the wall zones to correctly capture the velocity and pressure gradients near no-slip walls [21]. Hence, by creating automatic inflation using program controlled function in ANSYS Meshing, thin elements near wall can be created to capture normal gradient with minimal elements. The rest of the settings are set as default.

After choosing the above settings, mesh is generated for 3D model of PX-45S.

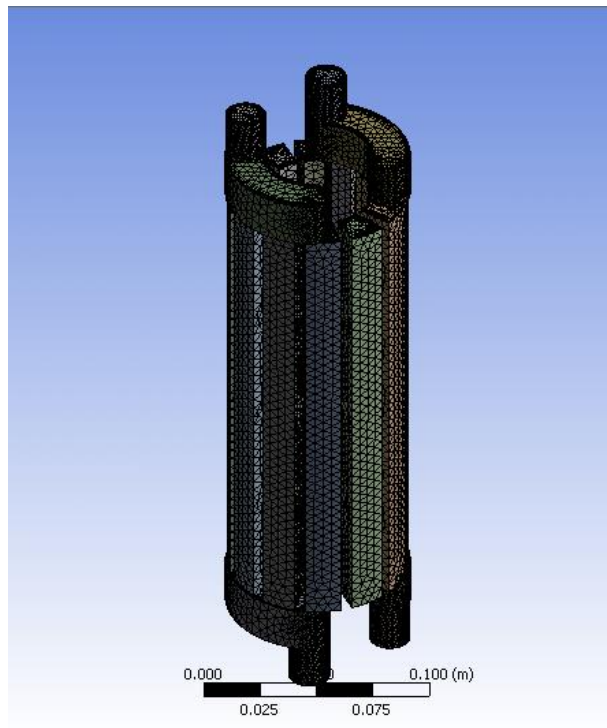


Figure 18. Meshing of Configuration 1 in ANSYS Meshing



Figure 19. Meshing of Configuration 2 in ANSYS Meshing

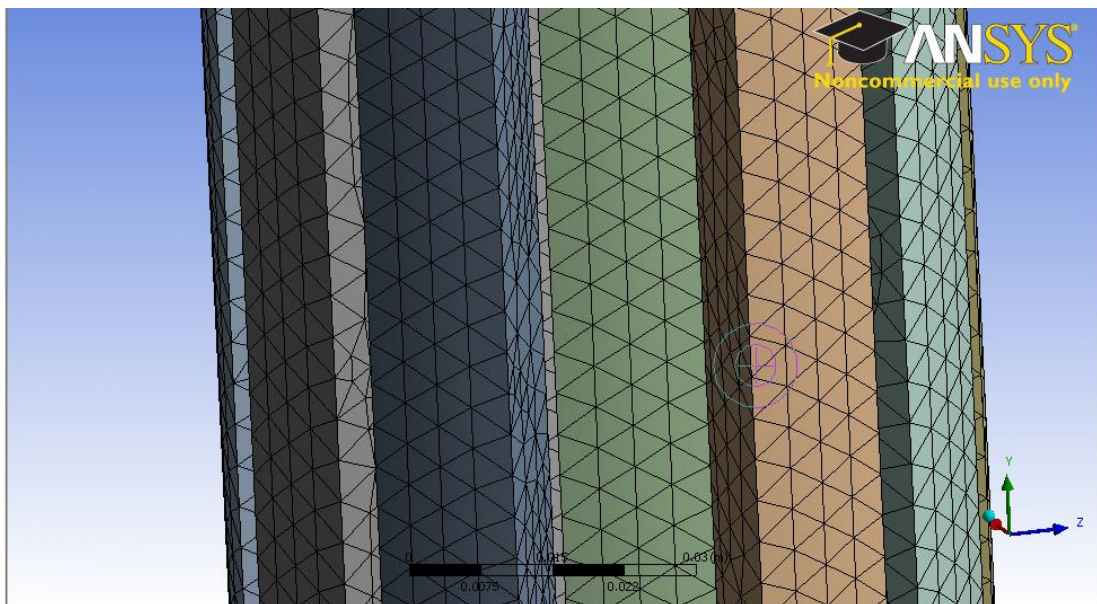


Figure 20. Zoom In View of Meshing of PX-45S in ANSYS Meshing

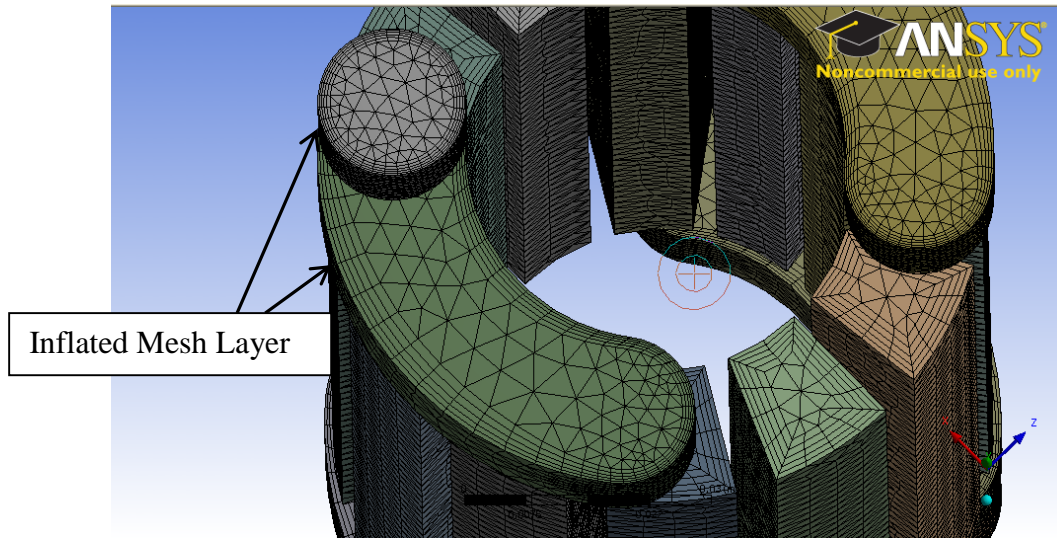


Figure 21. Inflated Layer of Meshing in ANSYS Meshing

Table 8 shows the statistics of the mesh generated on PX-45S single rotor pressure exchanger model in ANSYS Meshing:-

Table 8. Statistics of Configuration 1 Meshing

Statistics	Value
Nodes	99179
Elements	239204
Orthogonal Quality (Average)	0.836901659394807

Table 9. Statistics of Configuration 2 Meshing

Statistics	Value
Nodes	92073
Elements	211817
Orthogonal Quality (Average)	0.829412139422442

Orthogonal quality is used to determine the quality of mesh, with 0 as the lowest quality mesh and 1 as the highest quality. The orthogonal quality of mesh from the settings above is approximately 0.83 to 0.84 for both configurations, which is a good mesh for the model. Besides that, the number of elements is around

200,000, which is sufficient for the calculation and does not exceed 512,000 elements (Limit of ANSYS Fluent software with academic license).

4.3 ANSYS Fluent

Physics in ANSYS Fluent are setup according to section 3.5 Setup Physics. Below are the screenshots of setup settings:-

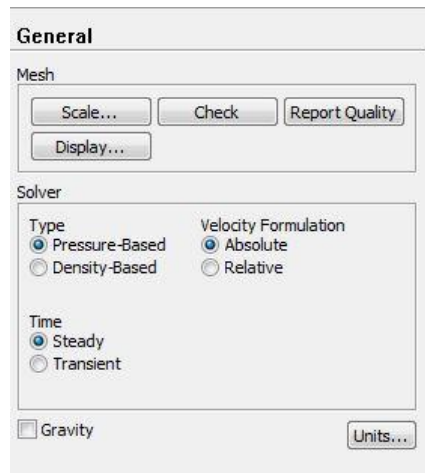


Figure 22. General Setup of ANSYS Fluent

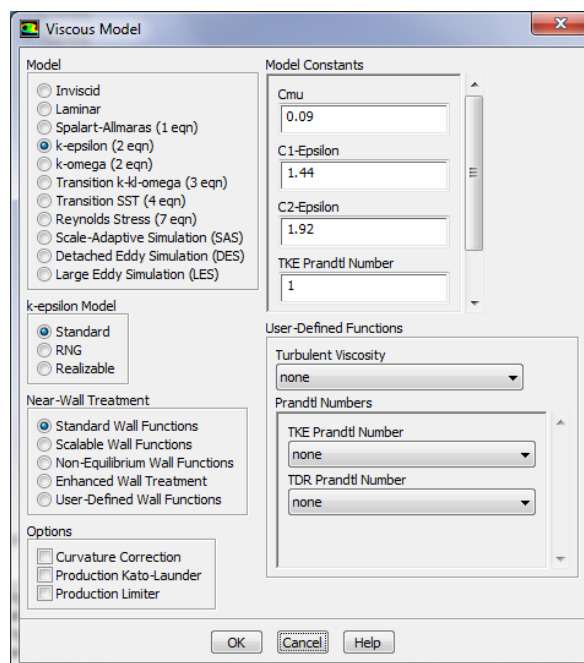


Figure 23. Viscous Model of ANSYS Fluent

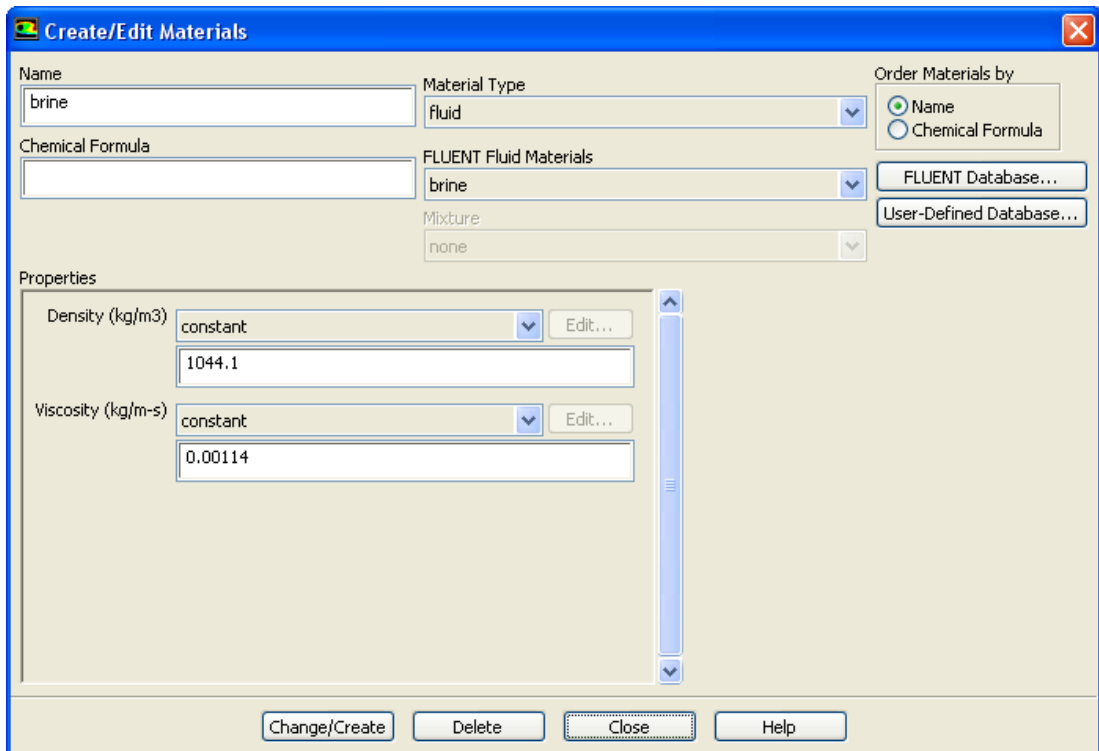


Figure 24. Material Setup (Brine) of ANSYS Fluent

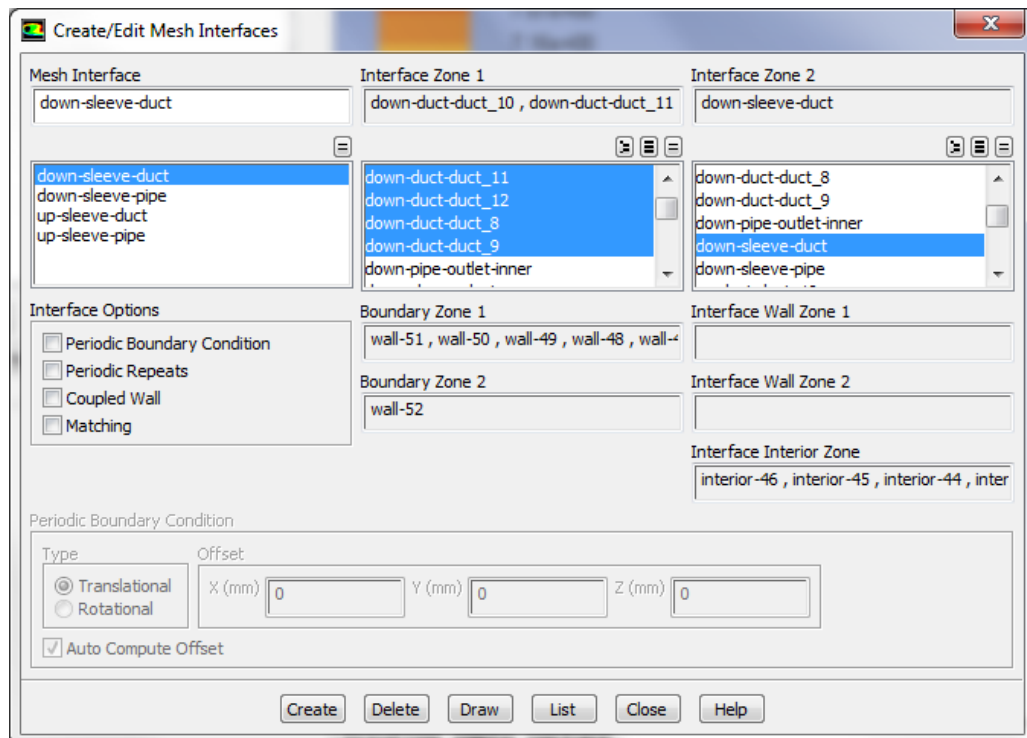


Figure 25. Mesh Interfaces

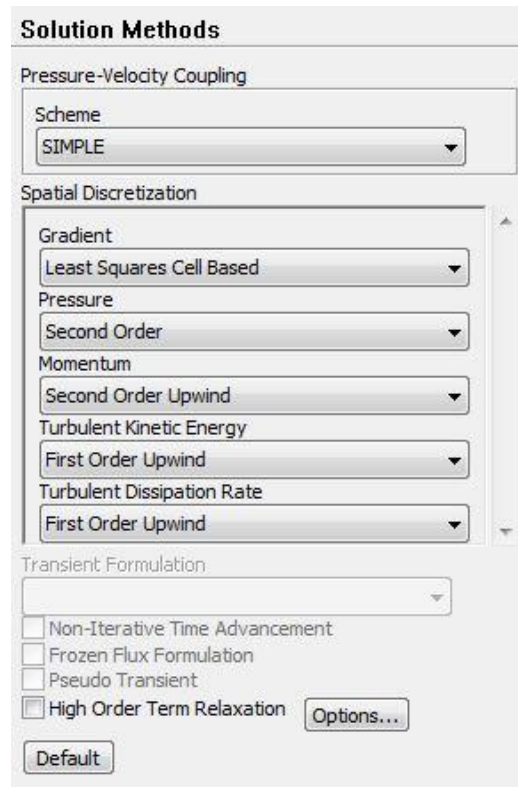


Figure 26. Solution Methods

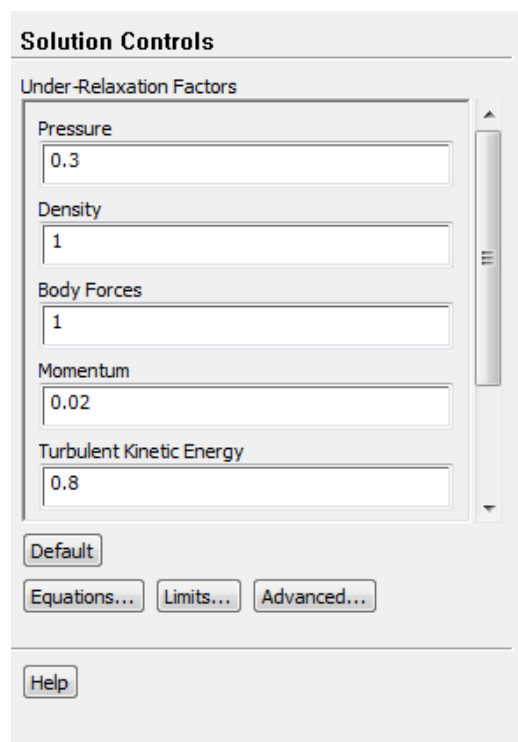


Figure 27. Solution Controls

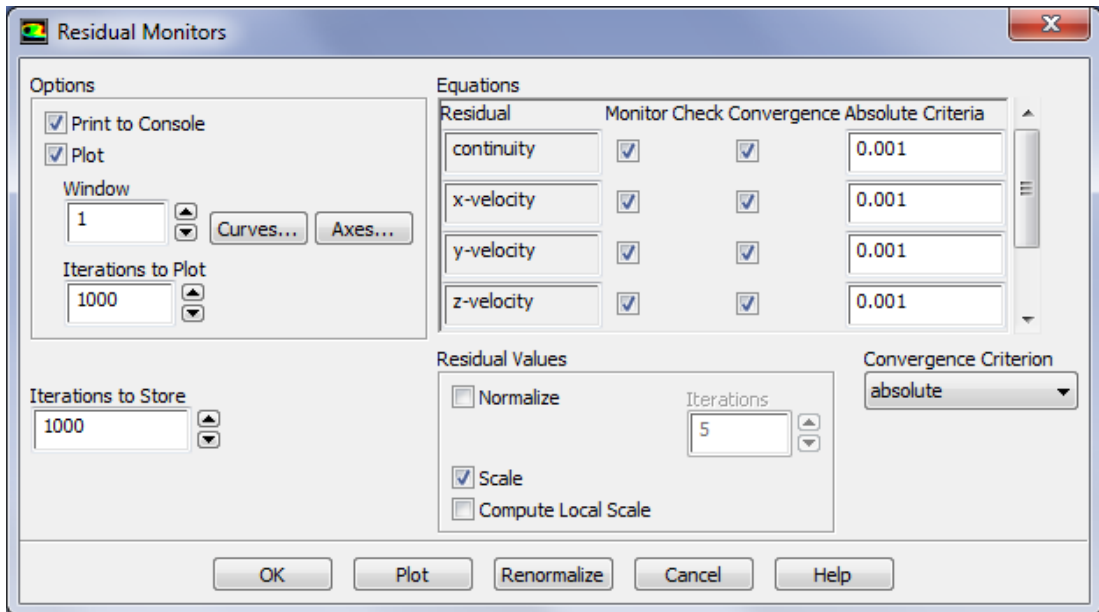


Figure 28. Residual Monitors

The same physics are setup for Configuration 1 and Configuration 2. After setting up physics, simulation is computed in ANSYS Fluent to study the computational fluid dynamics of PX-45S single rotor pressure exchanger. Below are the results of the simulation:-

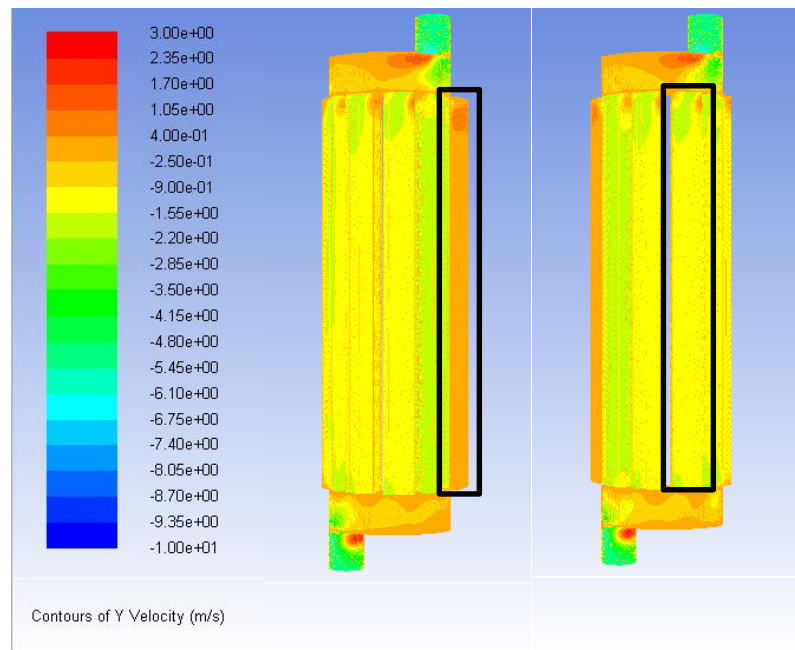


Figure 29. Velocity profile of Configuration 1 at 0ms and 8ms

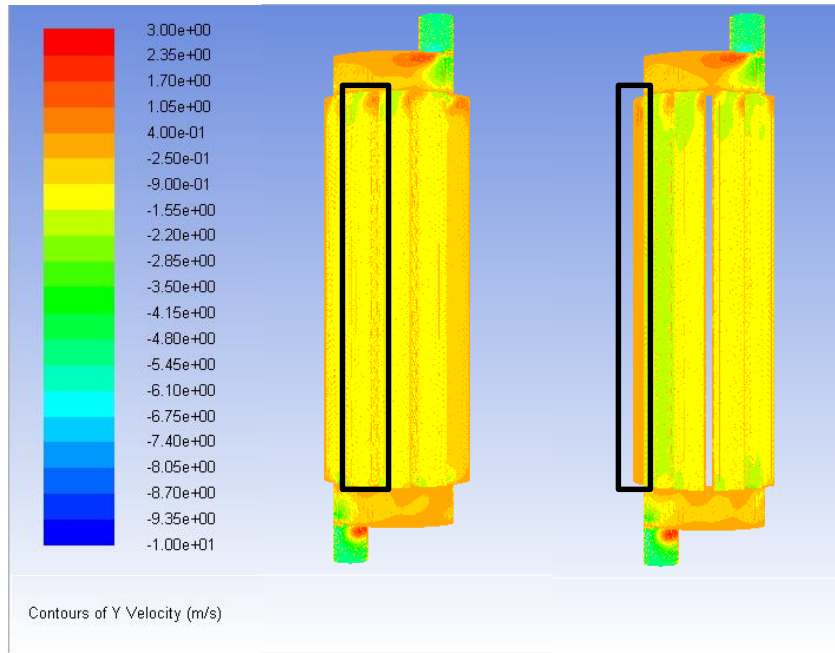


Figure 30. Velocity profile of Configuration 1 at 16ms and 23ms

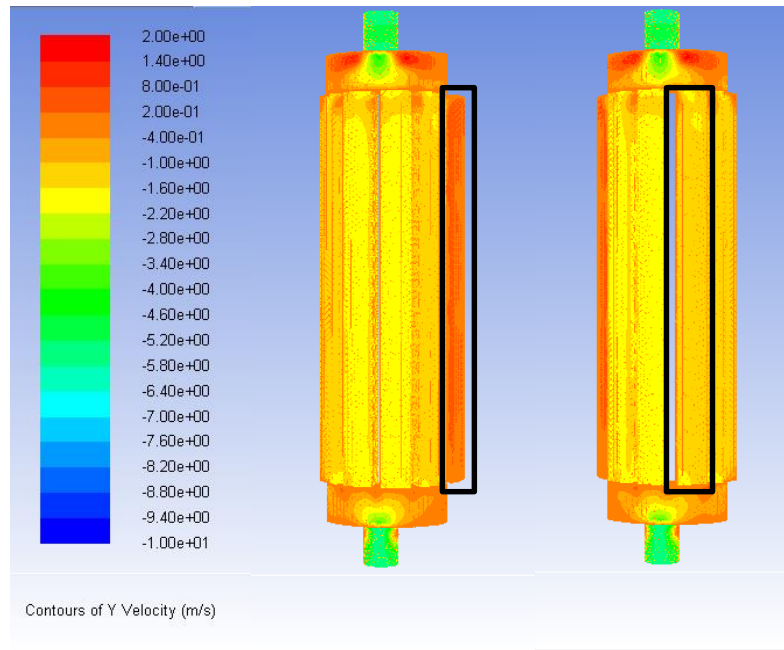


Figure 31. Velocity profile of Configuration 2 at 0ms and 8ms

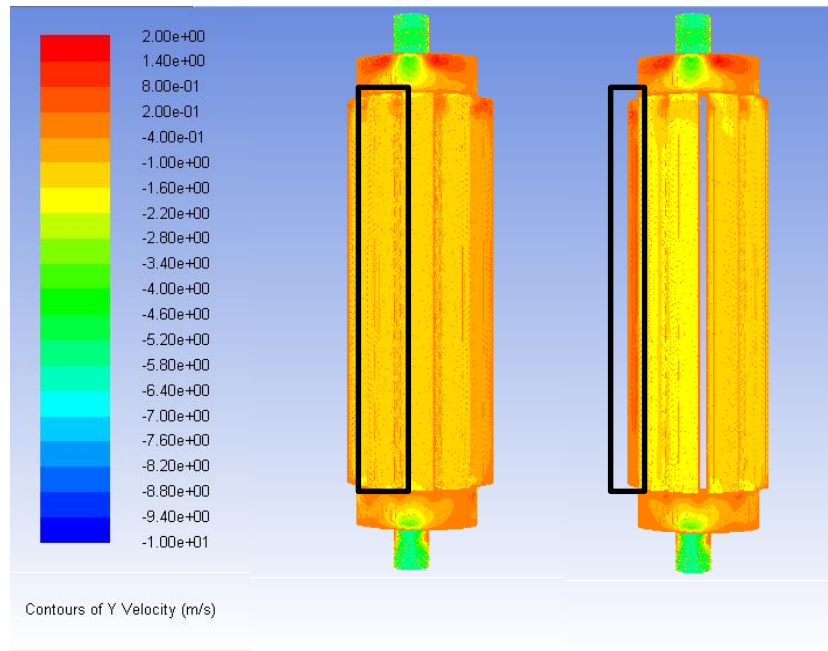


Figure 32. Velocity profile of Configuration 2 at 16ms and 23 ms

4.4 Discussion

The velocity profile is obtained in the previous sub chapter. Hence, volume-weighted average y-velocity of reference duct can be obtained. In this project, only y-velocity magnitude is considered as it is the effective velocity that brine solution flows across the duct. Below is a plot of y-velocity versus time graph in reference duct of Configuration 1 and Configuration 2.

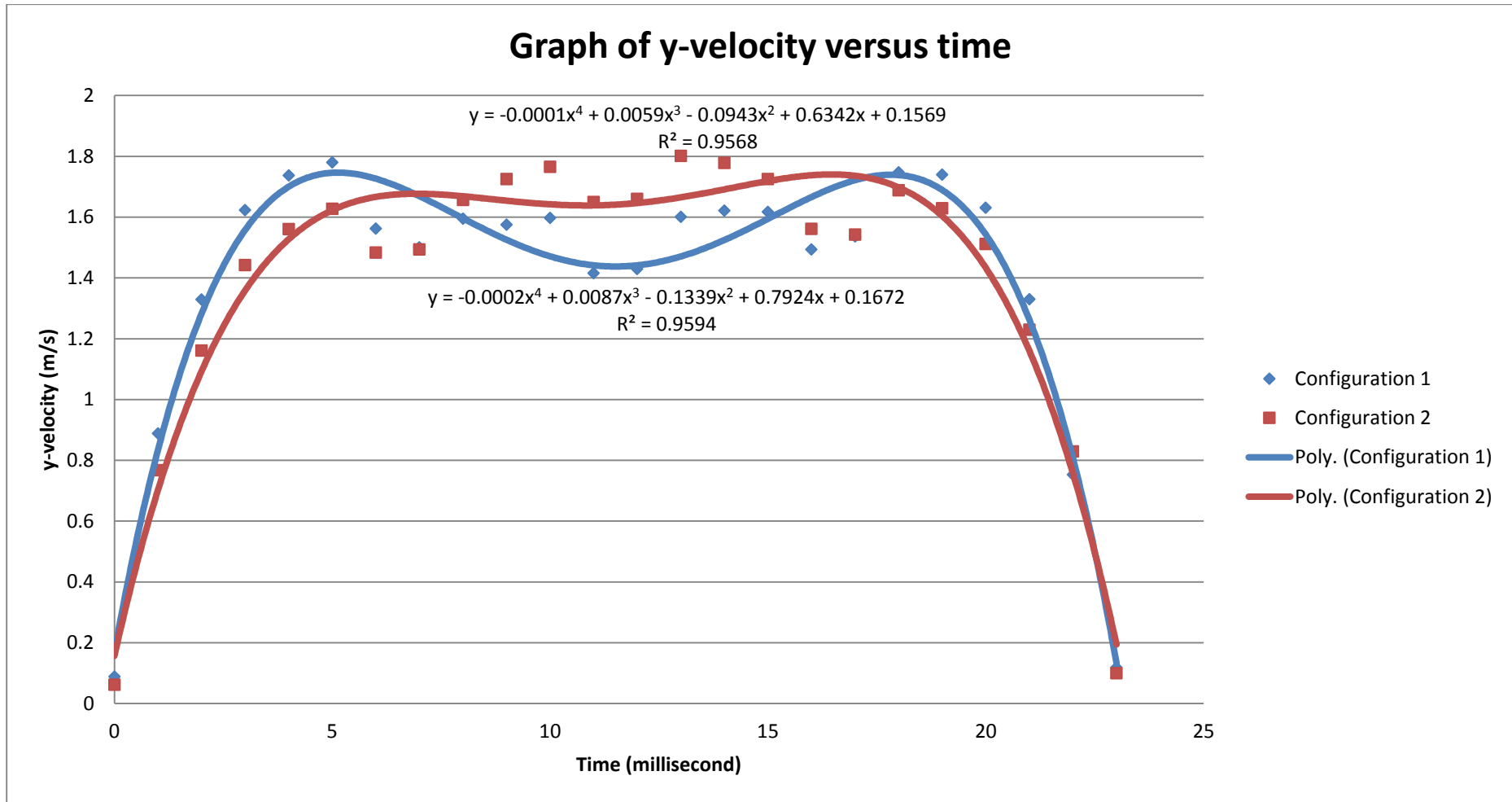


Figure 33: Graph of y-velocity versus time

Hence, from velocity obtained in ANSYS Fluent 15.0, pressure drop across the reference duct can be calculated using Darcy-Weisbach equation. The equation is as below[22]:-

$$\Delta P = \lambda \left(\frac{l}{d_h} \right) \left(\frac{\rho v^2}{2} \right) \quad (1)$$

Where,

ΔP = pressure loss (Pa)

λ = Darcy-Weisbach friction coefficient

l = length of duct (m)

d_h = hydraulic diameter (m)

ρ = density (kg/m³)

v = velocity (m/s)

Darcy-Weisbach friction coefficient can be calculated using Colebrook equation as below:-

$$\frac{1}{\lambda^{0.5}} = -2 \log \left[\left(\frac{2.51}{Re \cdot \lambda^{0.5}} \right) + \frac{k}{3.72 d_h} \right] \quad (13)$$

Where,

Re = Reynolds Number

k = roughness of duct (m)

The rotor is made up of stainless steel [23]. Hence, the roughness of duct is 0.015m [5].

Reynolds number can be calculated as below:-

$$Re = \frac{\rho v d_h}{\mu} \quad (14)$$

Where,

μ = dynamic viscosity (kg/m.s)

Hydraulic diameter can be calculated as below:-

$$d_h = \frac{4A}{p} = 0.016m \quad (15)$$

Where,

A = area section of duct (m²)

p = wetted perimeter of the duct (m)

Therefore, from using equations above, pressure drop across duct can be calculated.

Below are the tables with values for calculation of pressure drop:-

Table 10. Pressure drop values for Configuration 1

Time (millisecond)	Velocity (m/s)	Re	Lambda	Pressure Drop (Pa)
0	0.08852011	1297.176798	0.08	4.091
1	0.88827467	13016.80818	0.08	411.914
2	1.3294286	19481.49335	0.08	922.661
3	1.6235558	23791.64366	0.08	1376.089
4	1.736953	25453.37021	0.08	1575.028
5	1.779811	26081.41284	0.08	1653.712
6	1.562607	22898.49781	0.08	1274.711
7	1.5008291	21993.20229	0.08	1175.911
8	1.595176	23375.76508	0.08	1328.401
9	1.574765	23076.66156	0.08	1294.264
10	1.597653	23412.06312	0.08	1332.53
11	1.416076	20751.22739	0.08	1046.582
12	1.429156	20942.90217	0.08	1066.28
13	1.601018	23461.37395	0.08	1338.149
14	1.621403	23760.09645	0.08	1372.422
15	1.616897	23694.06537	0.08	1364.825
16	1.4933311	21883.32634	0.08	1164.191
17	1.5368987	22521.76748	0.08	1233.112
18	1.747512	25608.10216	0.08	1594.235
19	1.739477	25490.35699	0.08	1579.609
20	1.630633	23895.3532	0.08	1388.112
21	1.329994	19489.77874	0.08	923.446
22	0.752642	11029.24228	0.08	295.726
23	0.1184526	1735.808557	0.08	7.325

Table 11. Pressure drop values for Configuration 2

Time (millisecond)	Velocity (m/s)	Re	Lambda	Pressure drop (Pa)
0	0.06185961	906.4928955	0.08	1.998
1	0.7670709	11240.68388	0.08	37.173
2	1.161115	17015.01995	0.08	703.822
3	1.442491	21138.31373	0.08	1086.271
4	1.560597	22869.0432	0.08	1271.433
5	1.627169	23844.59162	0.08	1382.211
6	1.48366	21741.6057	0.08	1149.161
7	1.493785	21889.9778	0.08	1164.899
8	1.656415	24273.16353	0.08	1432.354
9	1.724792	25275.16249	0.08	1553.05
10	1.765556	25872.51957	0.08	1627.328
11	1.649736	24175.28923	0.08	1420.826
12	1.660048	24326.40164	0.08	1438.644
13	1.801704	26402.23363	0.08	1694.646
14	1.77804	26055.46055	0.08	1650.423
15	1.725335	25283.11963	0.08	1554.028
16	1.5612	22877.87958	0.08	1272.416
17	1.542735	22607.29282	0.08	1242.495
18	1.68802	24736.30431	0.08	1487.535
19	1.62926	23875.23321	0.08	1385.776
20	1.511702	22152.53415	0.08	1193.011
21	1.230032	18024.93209	0.08	789.851
22	0.8295643	12156.46436	0.08	359.263
23	0.09932104	1455.454005	0.08	5.15

Graph below shows the pressure drop across a duct in Configuration 1 and Configuration 2:-

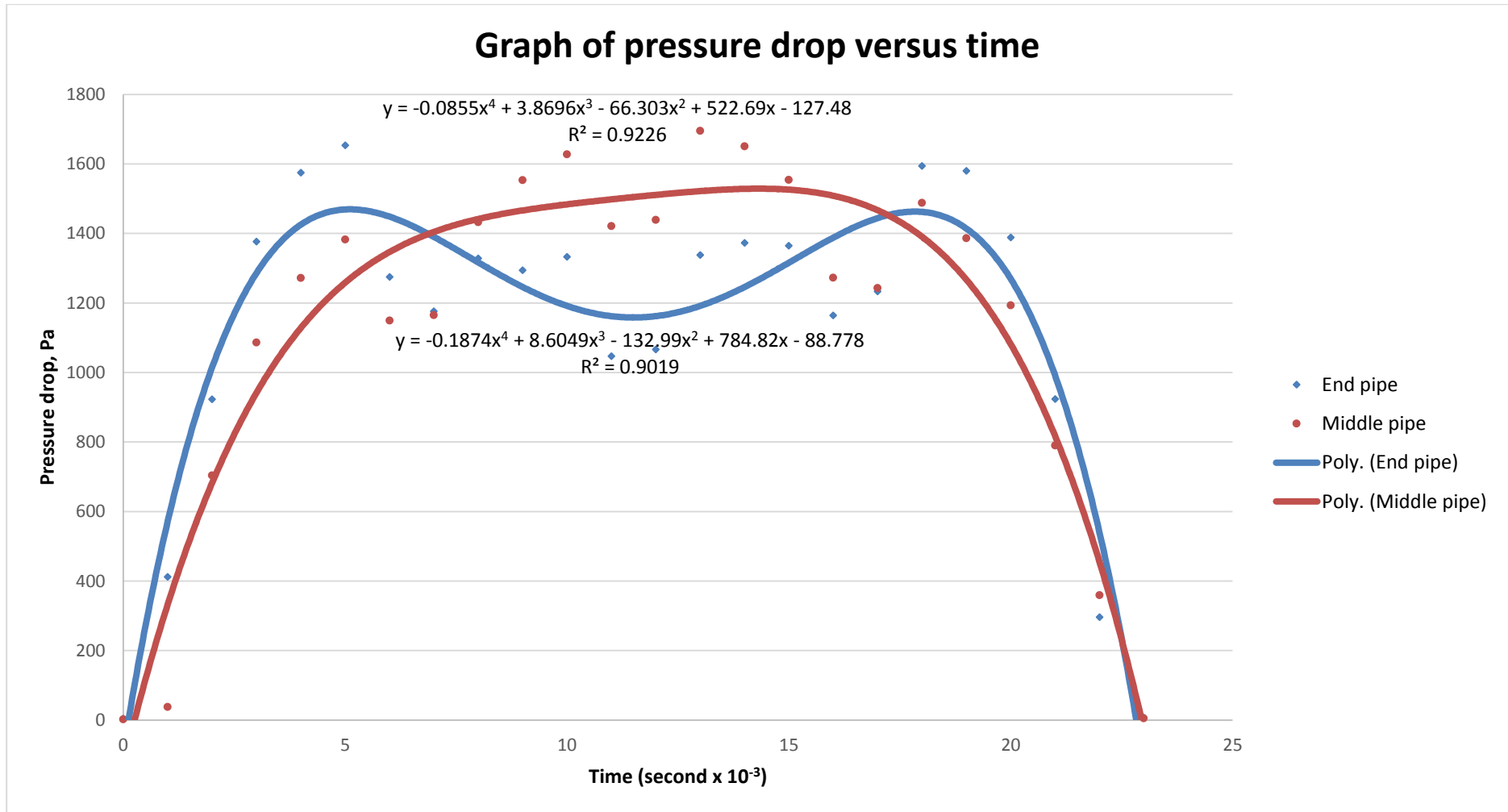


Figure 34. Graph of pressure drop versus time

From Figure 33 and Figure 34, it can be seen that Configuration 1 and Configuration 2 exhibit similar trends in both graphs, where plots of Configuration 1 shows “m”-shaped and plots of Configuration 2 shows inverted “u”-shaped.

For Configuration 1, the inlet and outlet pipes of the pressure exchanger are at both ends of the upper and lower sleeves. As the area of contact between reference duct and sleeve increases, more brine solution will flow into the reference duct. Hence, it shows an increasing trend in the early time frame. The y-velocity achieves highest for the first time when the reference duct is directly below the inlet pipe. As the reference duct rotates towards the middle of the sleeve, slight decrease can be seen in the volume-weighted average y-velocity in reference duct. Y-velocity in the reference duct achieves highest for second time when the reference duct is directly above the outlet pipe. As the reference duct rotates away from the sleeve, the y-velocity decreases sharply.

For Configuration 2, the inlet and outlet pipes of the pressure exchanger are at middle of the upper and lower sleeves. As the area of contact between reference duct and sleeve increases, more brine solution will flow into the reference duct. Hence, it shows an increasing trend in the early time frame. As the reference duct approaching middle of the sleeve, the volume-weighted average y-velocity shows a plateau. As the reference duct rotates away from the sleeve, the y-velocity decreases sharply.

Since plots of both configurations do not exhibit same trends, the configuration that has lower pressure drop cannot be identified solely from the graphs. Hence, the average pressure drop from 0ms to 23ms is calculated for Configuration 1 and Configuration 2.

The average pressure drop in Configuration 1 is 1113.472Pa and the average pressure drop in Configuration 2 is 1120.99Pa. Hence, Configuration 1 is slightly better than Configuration 2 by 0.7% in terms of pressure drop across a duct.

CHAPTER 5

CONCLUSION AND RECOMMENDATIONS

5.1 Conclusion

Development of pressure exchanger to recover waste pressure has played a significant role in sea water reverse osmosis process. Since pressure exchanger has only been used in industrial practice since late 1990's, researches conducted on pressure exchanger are limited. This is especially true for the computational fluid dynamics of a pressure exchanger.

Therefore, the CFD of pressure exchanger will be developed in this project using ANSYS Fluent 15.0 software. ANSYS Fluent is a sophisticated CFD simulation tool to study temperature, pressure and flow profile of a model. By developing equipment (PX-45S) based on the real dimension and geometry, the result of this model would be closely related to nowadays application. This simulation can then provide a platform for further researchers to conduct study on the possibility of usage of pressure exchanger in other fields and applications.

Based on the results and discussion, it can be seen that Configuration 1 has average pressure drop of 1113.472Pa and Configuration 2 has average pressure drop of 1120.99Pa at one time step. In conclusion, Configuration 1 is slightly better than Configuration 2 in terms of pressure drop by 0.7%. Hence, it can be concluded that possibility of enhancement of pressure exchanger by altering piping configurations is not feasible. Other approaches should be made to further improve the efficiency of pressure exchanger.

5.2 Recommendations

Below are some recommendations for future work relating to computational fluid dynamics (CFD) study of single rotor pressure exchanger:-

1. Study the effect of rotor rotational speed on the effect of pressure drop across duct.
2. Study the effect of mixing rate in the duct on the effect of pressure drop across duct.

REFERENCES

- [1] G. G. Pique, "SWRO Desalination: A Viable, Long-Term Solution to Water Scarcity," in *Environmental Protection*, 2010.
- [2] "ANSYS Fluent," in *ANSYS*, 2014.
- [3] "PX-S Series," in *Energy Recovery, Inc.*, 2014.
- [4] "PX-Q Series," in *Energy Recovery, Inc.*, 2014.
- [5] G. Brown, "The Darcy-Weisbach Equation," in *Henry Darcy and His Law*, 2000.
- [6] S. Mambretti, E. Orsi, S. Gagliardi, and R. Stover, "Behaviour of energy recovery devices in unsteady flow conditions and application in the modelling of the Hamma desalination plant," *Desalination* 238, pp. 233-245, 2009.
- [7] W. T. Andrews, W. F. Pergande, and G. S. McTaggart, "Energy performance enhancements of a 950m³/d seawater reverse osmosis unit in Grand Cayman," *Desalination* 135, pp. 195-204, 2001.
- [8] S. Bross and W. Kochanowski, "SWRO core hydraulic module - the right concept decides in terms of energy consumption and realibility Part II. Advanced pressure exchanger design," *Desalination* 165, pp. 351-361, 2004.
- [9] L. A. Pelton, US Patent 233,692, 1880.
- [10] R. L. Stover, "Development of a fourth generation energy recovery device. A 'CTO's Notebook'," *Desalination*, pp. 313-321, 2004.
- [11] L. J. Hauge, US Patent 4,887,942, 1989.
- [12] L. J. Hauge, "The pressure exchanger - A key to substantial lower desalination cost," *Desalination*, pp. 219-223, 1995.
- [13] C. M. Chiang, Y.-H. Liu, and A. W.-K. Law, "Theory of isobaric pressure exchanger for desalination," *Desalination and Water Treatment*, pp. 112-122, 2012.
- [14] J. P. MacHarg and S. A. McClellan, "Pressure Exchanger Helps Reduce Energy Costs in Brackish Water RO System," *AWWA*, pp. 44-47, 2004.
- [15] Y. Zhou, M. Bi, and Y. Liu, "Rotary Pressure Exchanger for SWRO," in *Expanding Issues in Desalination*, ed: InTech, 2011, pp. 103-120.
- [16] "Assy, S Series, 4" Single Rotor," ed. San Leandro, California, USA: Energy Recovery Inc., 2007.

- [17] "Darcy-Weisbach Formula,"
- [18] "Pressure Exchanger Specifications Sheet PX-45S," in *Technical Data Sheet, Positive Displacement Energy Recovery Device*, ed. San Leandro, California, USA: Energy Recovery, Inc., 2012.
- [19] "Reverse Osmosis Desalination: Brine disposal," in *Lenntech*
- [20] M. H. Sharqawy, J. H. L. V, and S. M. Zubair, *Thermophysical Properties of Seawater: A Review of Existing Correlations and Data, Desalination and Water Treatment*, 2010.
- [21] J. Chawner, "Accuracy, Convergence and Mesh Quality," in *Another Fine Mesh*, 2012.
- [22] "Tips & Tricks: Global Meshing Controls in ANSYS," in *Leap Australia Computational Fluid Dynamics Blog*, 2011.
- [23] "Top 5 Do's and Don'ts for CFD," in *SimuTech Group*, 2014.

Appendices

APPENDIX A: SEAWATER DENSITY CORRELATIONS

Table 2
Seawater density correlations.

Correlation

$$\rho_{sw} = 10^3 (A_1 F_1 + A_2 F_2 + A_3 F_3 + A_4 F_4)$$

where

$$B = (2S_p - 150)/150, G_1 = 0.5, G_2 = B, G_3 = 2B^2 - 1$$

$$A_1 = 4.032G_1 + 0.115G_2 + 3.26 \times 10^{-4}G_3$$

$$A_2 = -0.108G_1 + 1.571 \times 10^{-3}G_2 - 4.23 \times 10^{-4}G_3$$

$$A_3 = -0.012G_1 + 1.74 \times 10^{-3}G_2 - 9 \times 10^{-6}G_3$$

$$A_4 = 6.92 \times 10^{-4}G_1 - 8.7 \times 10^{-5}G_2 - 5.3 \times 10^{-5}G_3$$

$$A = (2t_{68} - 200)/160, F_1 = 0.5, F_2 = A, F_3 = 2A^2 - 1, F_4 = 4A^3 - 3A$$

Validity: ρ_{sw} in (kg/m³); $20 < t_{68} < 180$ °C; $10 < S_p < 160$ g/kg

Accuracy: ± 0.1 %

$$\rho_{sw} = \rho_w + A S_p + B S_p^{3/2} + C S_p^2$$

where

$$A = 0.824493 - 4.0899 \times 10^{-3}t_{68} + 7.6438 \times 10^{-5}t_{68}^2 - 8.2467 \times 10^{-7}t_{68}^3 + 5.3875 \times 10^{-9}t_{68}^4$$

$$B = -5.72466 \times 10^{-3} + 1.0227 \times 10^{-4}t_{68} - 1.6546 \times 10^{-6}t_{68}^2, C = 4.8314 \times 10^{-4}$$

$$\rho_w = 999.842594 + 6.793952 \times 10^{-2}t_{68} - 9.09529 \times 10^{-3}t_{68}^2 + 1.001685 \times 10^{-4}t_{68}^3 - 1.120083 \times 10^{-6}t_{68}^4 + 6.536336 \times 10^{-9}t_{68}^5$$

Validity: ρ_{sw} and ρ_w in (kg/m³); $-2 < t_{68} < 40$ °C; $0 < S_p < 42$ g/kg

Accuracy: ± 0.01 %

$$\rho_{sw} = \left(\begin{aligned} &a_1 + a_2t + a_3t^2 + a_4t^3 + a_5t^4 + a_6p + a_7pt^2 + a_8pt^3 + a_9pt^4 + a_{10}p^2 \\ &+ a_{11}p^2t + a_{12}p^2t^2 + a_{13}p^2t^3 + a_{14}p^3 + a_{15}p^3t + a_{16}p^3t^2 + a_{17}p^3t^3 + a_{18}p^3t^4 \end{aligned} \right) - (b_1S + b_2S t + b_3S t^2 + b_4S t^3 + b_5S p + b_6S p^2)$$

where

$$\begin{aligned} a_1 &= 9.992 \times 10^2, a_2 = 9.539 \times 10^{-2}, a_3 = -7.619 \times 10^{-3}, a_4 = 3.131 \times 10^{-5}, a_5 = -6.174 \times 10^{-8}, \\ a_6 &= 4.337 \times 10^{-1}, a_7 = 2.549 \times 10^{-5}, a_8 = -2.899 \times 10^{-7}, a_9 = 9.578 \times 10^{-10}, a_{10} = 1.763 \times 10^{-3}, \\ a_{11} &= -1.231 \times 10^{-4}, a_{12} = 1.366 \times 10^{-6}, a_{13} = 4.045 \times 10^{-9}, a_{14} = -1.467 \times 10^{-5}, a_{15} = 8.839 \times 10^{-7} \\ a_{16} &= -1.102 \times 10^{-9}, a_{17} = 4.247 \times 10^{-11}, a_{18} = -3.959 \times 10^{-14}, b_1 = -7.999 \times 10^{-1}, b_2 = 2.409 \times 10^{-3} \\ b_3 &= -2.581 \times 10^{-5}, b_4 = 6.856 \times 10^{-8}, b_5 = 6.298 \times 10^{-4}, b_6 = -9.363 \times 10^{-7} \end{aligned}$$

Validity: ρ_{sw} in (kg/m³); $0 < t < 180$ °C; $0 < S < 80$ g/kg; $0.1 < p < 100$ MPa

Accuracy: ± 2.5 %

$$\rho_{sw} = (a_1 + a_2t + a_3t^2 + a_4t^3 + a_5t^4) + (b_1S + b_2S t + b_3S t^2 + b_4S t^3 + b_5S^2t^2)$$

where

$$\begin{aligned} a_1 &= 9.999 \times 10^2, a_2 = 2.034 \times 10^{-2}, a_3 = -6.162 \times 10^{-3}, a_4 = 2.261 \times 10^{-5}, a_5 = -4.657 \times 10^{-8}, \\ b_1 &= 8.020 \times 10^2, b_2 = -2.001, b_3 = 1.677 \times 10^{-2}, b_4 = -3.060 \times 10^{-5}, b_5 = -1.613 \times 10^{-5} \end{aligned}$$

Validity: ρ_{sw} in (kg/m³); $0 < t < 180$ °C; $0 < S < 0.16$ kg/kg

Accuracy: ± 0.1 %

APPENDIX B: SEAWATER DYNAMIC VISCOSITY CORRELATIONS

Table 5
Seawater dynamic viscosity correlations.

Correlation

$$\log_{10} \left(\frac{\mu_{sw}}{\mu_w} \right) = 0.0428I + 0.00123I^2 + 0.000131I^3 + (-0.03724I + 0.01859I^2 - 0.00271I^3) \log_{10} (10^3 \times \mu_w)$$

where

μ_w is the pure water viscosity in (kg/m s) given by Dorsey [68]

I is the ionic strength given by $I = 19.915 S_p / (1 - 1.00487 S_p)$

Validity: $20 < t < 150^\circ\text{C}$; $15 < S_p < 130$

Accuracy: $\pm 0.4\%$

$$\mu_{sw} = \mu_w (1 + A Cl^{1/2} + B Cl)$$

$$A = 5.185 \times 10^{-5} t_{68} + 1.0675 \times 10^{-4} \quad \text{and} \quad B = 3.300 \times 10^{-5} t_{68} + 2.591 \times 10^{-3}$$

Cl is the volume chlorinity which is related to salinity by $Cl = \rho_{sw} S_p / 1806.55$

μ_w is the pure water viscosity in (kg/m s) given by Korson et al. [70]

$$\log_{10} (\mu_w / \mu_{20}) = (1.1709 (20 - t_{68}) - 0.001827 (t_{68} - 20)^2) / (t_{68} + 89.93)$$

μ_{20} is the viscosity of distilled water at 20°C which is equal to 1.002×10^{-3} kg/m.s (Swindells et al. [71]).

Validity: μ_{sw} in (kg/m.s); $5 < t_{68} < 25^\circ\text{C}$; $0 < S_p < 40$ g/kg

Accuracy: $\pm 0.5\%$

$$\mu_{sw} = \mu_w (1 + A S_p + B S_p^2)$$

$$A = 1.474 \times 10^{-3} + 1.5 \times 10^{-5} t_{68} - 3.927 \times 10^{-8} t_{68}^2$$

$$B = 1.073 \times 10^{-5} - 8.5 \times 10^{-8} t_{68} + 2.230 \times 10^{-10} t_{68}^2$$

μ_w is the pure water viscosity given by Korosi and Fabuss [72]

Validity: μ_{sw} in (kg/m.s); μ_w in (kg/m.s); $10 < t_{68} < 180^\circ\text{C}$; $0 < S_p < 150$ g/kg

Accuracy: $\pm 1\%$

$$\mu_{sw} = \mu_w (1 + A S + B S^2)$$

$$A = 1.541 + 1.998 \times 10^{-2} t - 9.52 \times 10^{-5} t^2$$

$$B = 7.974 - 7.561 \times 10^{-2} t + 4.724 \times 10^{-4} t^2$$

μ_w is based on the IAPWS 2008 [73] data and given by

$$\mu_w = 4.2844 \times 10^{-5} + (0.157 (t + 64.993)^2 - 91.296)^{-1}$$

Validity: μ_{sw} and μ_w in (kg/m.s); $0 < t < 180^\circ\text{C}$; $0 < S < 0.15$ kg/kg

Accuracy: $\pm 1.5\%$